RM No. E7D04

RESEARCH MEMORANDUM

for the

Bureau of Aeronautics, Navy Department

ALTTITUDE-WIND-TUNNEL INVESTIGATION OF THE 19B-2, 19B-8 AND 19XB-1 JET-PROPULSION ENGINES

IV - ANALYSIS OF COMPRESSOR PERFORMANCE

By Robert O. Dietz and John K. Kuenzig

Aircraft Engine Research Laboratory
Cleveland, Ohio

NATIONAL ADVISORY COMMITTEE
FOR AERONAUTICS

WASHINGTON

APR 25 1947

NACA RM No. E7D04

NATIONAL ADVISORY COMMITTEE FOR AERONAUTICS

RESEARCH MEMORANDUM

for the

Bureau of Aeronautics, Navy Department

ALTITUDE-WIND-TUNNEL INVESTIGATION OF THE 19B-2, 19B-8 AND 19XB-1 JET-PROPULSION ENGINES

IV - ANALYSIS OF COMPRESSOR PERFORMANCE

By Robert O. Dietz and John K. Kuenzig

SUMMARY

Investigations were conducted in the Cleveland altitude wind tunnel to determine the performance and operational characteristics of the 19B-2, 19B-8, and 19XB-1 turbojet engines. One objective was to determine the effect of altitude, flight Mach number, and tail-pipe-nozzle area on the performance characteristics of the six-stage and ten-stage axial-flow compressors of the 19B-8 and 19XB-1 engines, respectively.

The data were obtained over a range of simulated altitudes and flight Mach numbers. At each simulated flight condition the engine was run over its full operable range of speeds. Performance characteristics of the 19B-8 and 19XB-1 compressors for the range of operation obtainable in the turbojet-engine installation are presented. Compressor characteristics are presented as functions of air flow corrected to sea-level conditions, compressor Mach number, and compressor load coefficient.

For the range of compressor operation investigated, changes in Reynolds number had no measurable effect on the relations among compressor Mach number, corrected air flow, compressor load coefficient, compressor pressure ratio, and compressor efficiency. The operating lines for the 19B-8 compressor lay on the low-air-flow side of the region of maximum compressor efficiency; the 19B-8 compressor operated at higher average pressure coefficients per stage and produced a lower over-all pressure ratio than did the 19XB-1 compressor.

INTRODUCTION

Compressor performance data have been obtained from an investigation of the complete 19B-2, 19B-8, and 19XB-1 turbojet engines over a wide range of simulated flight conditions in the Cleveland altitude wind tunnel. Operational characteristics of all three engines are presented in reference 1; performance characteristics of the 19B-8 and 19XB-1 engines are presented in reference 2; and turbine performance characteristics of the 19B-8 engine are presented in reference 3. Compressor performance characteristics for the 19B-8 and 19XB-1 engines over a range of simulated flight conditions are presented herein. No data for the 19B-2 engine are given inasmuch as the 19B-2 and 19B-8 compressors are similar.

Compressor characteristics were investigated to determine the effects of altitude, flight Mach number, and tail-pipe-nozzle area on compressor performance and to determine how effectively the compressors were used in these engines.

The performance of the compressors is presented as a function of air flow corrected to sea-level conditions, compressor Mach number, and compressor load coefficients. The data presented were obtained at simulated altitudes of 5000, 20,000, and 25,000 feet; at flight Mach numbers, based on free-stream total and static pressures, from 0.03 to 0.317; and at compressor Mach numbers from 0.470 to 1.150. Data for the 19B-8 compressor are compared with the results of standard dynamometer tests of the compressor presented in reference 4.

DESCRIPTION OF COMPRESSORS

The 19B-8 compressor is a six-stage axial-flow type designed to handle 28 pounds of air per second at an engine speed of 17,500 rpm at standard sea-level conditions. The 19XB-1 compressor is a ten-stage axial-flow type designed to handle 29 pounds of air per second at an engine speed of 16,500 rpm at standard sea-level conditions. These compressors have five principal components: inlet section, split stator casing, rotor, blading, and discharge section. The relation among the parts of the compressor installation is shown in figure 1, which is taken from a Westinghouse installation manual. The length of the compressors from the front face of the front flange of the inlet section to the rear face of the rear flange of the discharge section is 32.40 inches and the outside diameter is 18.75 inches.

Streamlined struts in the inlet section support the front bearing and house the accessory drive shaft and the oil lines to the front

compressor bearing. The inside diameter of the inlet section increases from 14.5 inches at the upstream flange to 15.75 inches at the downstream flange. The inlet sections of the two engines are the same.

Aluminum stator casings containing the stator blading are the split type, which makes the blading accessible. Over the entire length of the blading, the casings have a constant inner diameter of 15.75 inches and diverge slightly at the discharge end to form diffuser sections. The stator blades are completely shrouded at the tips. These shrouds fit into grooves in the compressor rotor to form labyrinth seals that prevent leakage around the stator-blade tips. The stator casing also contains the compressor-inlet turning vanes and the compressor-outlet straightening vanes.

The rotor spindle is tapered to form a converging passage. Diameters of the 19B-8 and 19XB-1 compressor rotors are 9.1 inches at the upstream face and 12.5 and 12.75 inches, respectively, at the downstream face. Both the 19B-8 six-stage compressor and the 19XB-1 ten-stage compressor are the same length. The rotor blades are machined steel mounted on the rotor by a dovetail joint and locked in place by a wire key.

The discharge section contains eight streamlined struts that support the thrust bearing. The fuel-nozzle manifold is also housed in this section.

INSTALLATION AND DESCRIPTION OF ENGINES

The 19B-8 and 19XB-1 turbojet engines were installed in the 20-foot-diameter test section of the altitude wind tunnel in a stub-wing nacelle cantilevered from one side of the test section. (See fig. 2.) In figure 2(c) the inlet screen has been removed in order to show the compressor-inlet turning vanes.

A wooden cowl was installed on the front of the unit and the engine was completely enclosed in a streamlined nacelle (fig. 2(a)). In order to protect the compressor from flying objects in the tunnel, a 6-mesh wire screen was bolted to the front flange of the oil cooler 32.75 inches upstream of the first row of turning vanes in the compressor.

The 19B-8 engine has a maximum diameter of $20\frac{3}{4}$ inches, is $104\frac{1}{2}$ inches long, and weighs approximately 825 pounds. The component

parts of this engine are a six-stage axial-flow compressor, an annular combustion chamber, a single-stage turbine, a tail-pipe nozzle, and an adjustable tail cone for varying the tail-pipe-nozzle area. The tail-pipe-nozzle area can be varied from 135 to 106 square inches by moving the adjustable tail cone out.

The over-all dimensions and the component parts of the 19XB-1 engine are similar to those of the 19B-8 engine except that the compressor has ten axial-flow stages and the tail-pipe nozzle is fixed. The area of the tail-pipe nozzle on this engine is 103 square inches. The turbine and the turbine nozzles of the 19XB-1 turbojet engine, although similar in design to those in the 19B-8 engine, were so modified that sufficient power would be available from the turbine to drive the ten-stage axial-flow compressor.

A longitudinal section of the engine showing the stations at which pressure and temperature surveys were taken and the designation of the stations is shown in figure 3. A photograph of the rakes installed at the compressor inlet (station 2) and the compressor outlet (station 3) is shown in figure 4, and cross-sectional drawings of these stations showing the location of the instrumentation are shown in figures 5 and 6.

Two rakes, each at an angle of 45° with the vertical center line of the engine, were installed at the cowl-inlet station about $2\frac{7}{8}$ inches ahead of the front flange of the oil cooler. These rakes had 16 total-pressure tubes, 9 static-pressure tubes, and 4 thermocouples and were used to measure the air flow through the engine.

RANGE OF INVESTIGATION

The 19B-8 engine was operated over a range of simulated altitudes from 5000 to 25,000 feet, flight Mach numbers from 0.03 to 0.317, and tail-cone positions of 0 and 4 inches out. The 19XB-1 engine was operated at static test conditions over a range of simulated altitudes from 5000 to 25,000 feet. Because of the ejector effect of the turbojet-engine exhaust in the tunnel test section and the velocity induced by the tunnel exhauster scoop, the flight Mach number was approximately 0.03 during static tests.

SYMBOLS

The following symbols and necessary values are used in the analysis and figures:

A	cross-sectional area, square feet
a	velocity of sound, based on total temperature, feet per second
c_p	specific heat at constant pressure, 0.24 Btu per pound $^{\circ}R$
D	compressor rotor-blade tip diameter, feet
g	ratio of absolute to gravitational units of mass, 32.17
J	mechanical equivalent of heat, 778 foot-pounds per Btu
M	Mach number
N	engine speed, rpm
n	number of stages
P	total pressure, pounds per square foot absolute
p	static pressure, pounds per square foot absolute
Q	air flow, cubic feet per second
R	gas constant, 53.3 foot pounds per pound $^{\circ}R$
T	total temperature, $^{\circ}R$
T_i	indicated temperature, $^{\circ}R$
t	static temperature, $^{\circ}R$
U	rotor tip speed, feet per second
V	velocity, feet per second
W_a	air flow, pounds per second
α	thermocouple impact-recovery factor, 0.85

γ ratio of specific heats at constant pressure and constant volume

δ ratio of absolute total pressure at compressor inlet to absolute static pressure of NACA standard atmosphere at sea level ($P_2/2116$ pounds per square foot absolute)

η compressor adiabatic temperature-rise efficiency

θ ratio of absolute total temperature at compressor inlet to absolute static temperature of NACA standard atmosphere at sea level ($T_2/519\ ^{\circ}R$)

ρ mass density of air, slugs per cubic feet

Ψ average compressor pressure coefficient per stage

$N/\sqrt{\theta}$ engine speed corrected to NACA standard atmospheric conditions at sea level, rpm

$W_a\sqrt{\theta}/\delta$ air flow corrected to NACA standard atmospheric conditions at sea level, pounds per second

Subscripts:

0 free stream

1 cowl inlet

2 compressor inlet

3 compressor outlet

4 turbine inlet

c compressor

n turbine-nozzle throat

METHODS OF CALCULATION

The equations and the relations used to calculate the compressor performance parameters are summarized.

Static temperatures were calculated from indicated temperature readings by

$$t = \frac{T_i}{1 + \alpha\left[\left(\frac{P}{p}\right)^{\frac{\gamma - 1}{\gamma}} - 1\right]}$$

Total temperature was then found from the adiabatic relation

$$\frac{T}{t} = \left(\frac{P}{p}\right)^{\frac{\gamma - 1}{\gamma}}$$

Air flow through the compressor was calculated from pressure and temperature measurements at the cowl inlet (station 1) by

$$W_a = g\rho_1 A_1 V_1 = g\rho_1 A_1 \sqrt{2Jgc_p t_1\left[\left(\frac{P_1}{p_1}\right)^{\frac{\gamma_1 - 1}{\gamma_1}} - 1\right]}$$

Values of static pressure used in this equation were obtained by weighting the values of static pressure obtained at the cowl inlet with respect to area. Temperatures and total pressures were taken as the mathematical averages of the values obtained at the cowl inlet.

Compressor Mach number is defined as the dimensionless ratio

$$M_c = \frac{U}{a_2} = \frac{\pi DN}{60\sqrt{\gamma_2 gRT_2}}$$

The compressor load coefficient, which is a measure of the angle of attack of the compressor blading, is obtained from

$$\frac{Q_2}{ND^3} = \frac{60\ W_a}{\rho_2 ND^3}$$

The following equation was used to calculate the adiabatic temperature-rise efficiency:

$$\eta = \frac{\left[\left(\frac{P_3}{P_2}\right)^{\frac{\gamma_c - 1}{\gamma_c}} - 1\right]}{\left(\frac{T_3}{T_2}\right) - 1}$$

where γ_c is the ratio of specific heats corresponding to the average total temperature of the air flowing through the compressor $(T_3 + T_2)/2$.

The average compressor pressure coefficient per stage, which is a measure of the effectiveness of the compressor blading, was calculated by

$$\Psi = \frac{2}{n(\gamma_c - 1)} \frac{\left[\left(\frac{P_3}{P_2}\right)^{\frac{\gamma_c - 1}{\gamma_c}} - 1\right]}{M_c^2}$$

Flight Mach number was calculated by use of the equation

$$M_0 = \sqrt{\frac{2}{\gamma_0 - 1}\left[\left(\frac{P_0}{p_0}\right)^{\frac{\gamma_0 - 1}{\gamma_0}} - 1\right]}$$

RESULTS AND DISCUSSION

Theory of Presentation

Complete compressor characteristics such as those presented for the 19B compressor in reference 4 are obtained in standard compressor tests by varying the air flow at each rotational speed. In the altitude-wind-tunnel investigation, the compressors were tested as an integral part of turbojet engines; therefore a considerable variation of the air flow at a given engine speed was impossible. Over-all operating characteristics of the engine determine an operating line that represents the relation of the compressor pressure ratio to the corrected air flow when the engine speed is varied.

The position of the operating line with respect to the coordinates is primarily determined by the turbine-nozzle area and the ratio of the gas temperature at the turbine inlet to the temperature of the air at the compressor inlet when the pressure ratio across the turbine nozzles is greater than critical (approximately 1.89). Under these conditions the air flow through the compressor is approximately

$$W_a = \frac{K A_n P_4 \sqrt{\gamma_4}}{\sqrt{T_4}}$$

where K is a factor that is practically independent of temperature. From this equation and the definitions of θ and δ, the approximate corrected air flow $W_a \sqrt{\theta}/\delta$ is given by the equation

$$\frac{W_a \sqrt{\theta}}{\delta} = K_1 A_n \frac{\frac{P_4 \sqrt{\gamma_4}}{P_2}}{\sqrt{\frac{T_4}{T_2}}} \qquad (1)$$

where $K_1 = K \frac{2116}{\sqrt{519}}$

The loss in total pressure between the compressor outlet (station 3) and the turbine inlet (station 4) is small relative to the total pressures; therefore, P_4/P_2 in equation (1) may be approximated by the compressor pressure ratio P_3/P_2. It may then be seen that the only operational variable that affects the relation of corrected air flow to compressor pressure ratio is the ratio of the gas temperature at the turbine inlet to the temperature of the air at the compressor inlet. When the pressure ratio across the turbine nozzles is less than critical, in addition to these factors, the back pressure on the turbine nozzle influences the corrected air flow.

In addition to the relation between corrected air flow and compressor pressure ratio, the operating line may be represented by the relation between compressor pressure ratio and compressor Mach number and by the relation between compressor pressure ratio and compressor load coefficient.

Because the flight Mach numbers presented are based on measurements of free-stream total pressure, the losses in the cowl inlet must be considered in determining the actual simulated flight conditions at the compressor inlet. The screen installed at the cowl

inlet by NACA for the wind-tunnel investigation caused a total-pressure loss between the free stream and the compressor inlet that varied with corrected engine speed. The relation between the ratio of compressor-inlet total pressure to free-stream total pressure and corrected engine speed for a range of flight Mach numbers and simulated altitudes is shown in figure 7.

Position of Operating Line

Effect of altitude. - The effect of simulated altitude on the operating line of each compressor is negligible (fig. 8). This absence of an altitude effect indicates that Reynolds number has no appreciable effect upon the compressor operating line. Unpublished data show that, for the range of altitudes investigated, variations of the ratio of gas temperature at the turbine inlet to the temperature of the air at the compressor inlet T_4/T_2 (equation (1)) is negligible in the range where the pressure drop across the turbine nozzles is critical.

The maximum corrected air flows observed for the 19B-8 and 19XB-1 compressors operating in their respective engines at static conditions were 30.4 and 27.3 pounds per second, respectively (fig. 8(a)). Corrected air flow of the 19B-8 engine at corrected rated engine speed ($N/\sqrt{\theta}$ = 17,500 rpm) with tail cone in and static test conditions was 29.4 pounds per second. (See figs. 8(a) and 8(b).) Maximum allowable turbine temperatures limited the 19XB-1 engine to rotational speeds below the rated value of 16,500 rpm. The maximum corrected engine speed obtained at static conditions was 16,250 rpm with a corrected air flow of 27.3 pounds per second. (See figs. 8(a) and 8(b).)

Effect of flight Mach number. - The effect of flight Mach number on the compressor operating line of the 19B-8 engine is shown in figure 9. No curve is presented for the 19XB-1 engine because it was operated only at static conditions. The increase in air flow that accompanies an increase in flight Mach number at a given compressor pressure ratio and turbine-nozzle Mach number of 1 is explained by equation (1). From this equation it can be seen that a decrease in the value of T_4/T_2 would be accompanied by an increase in air flow. From analysis and unpublished data it was found that an increase in flight Mach number was accompanied by a decrease in the value of T_4/T_2. When the turbine-nozzle Mach number is less than 1, the effective decrease in the back pressure on the turbine accompanied by an increase in flight Mach number is an additional factor affecting the increase in air flow.

Effect of tail-cone position. - A decrease in tail-pipe-nozzle area (that is, moving the tail cone out) of the 19B-8 engine increases the back pressure on the turbine. If the inlet conditions remain unchanged, the decrease in tail-pipe-nozzle area is equivalent to lowering the pressure altitude and decreasing the flight Mach number at a given air flow so far as the internal engine components are concerned. Inasmuch as altitude has no effect on the compressor operating line, moving the tail cone out has approximately the same effect on performance at a given air flow as that produced by a decrease in flight Mach number. Figure 10 shows the effect of tail-cone position on the compressor operating line.

Efficiencies

Effects of flight Mach number, tail-cone position, and simulated altitude on the 19B-8 compressor efficiency are shown in figure 11(a) where one curve is drawn through all the data points. The points were plotted in one figure to show that the random scatter of the efficiency data is sufficient to conceal any effect of flight Mach number, tail-cone position, and altitude that might be present. In figure 11(b), static-test data obtained at three altitudes for the 19XB-1 compressor are similarly treated.

The maximum efficiency for both compressors was approximately 81.5 percent. The conditions at maximum efficiency and at rated corrected engine speed for static conditions are presented for both compressors in the following table:

Compressor	Conditions	Corrected engine speed $N/\sqrt{\theta}$ (rpm)	Tail-cone position (in. out)	Corrected air flow $W\sqrt{\theta}/\delta$ (lb/sec)	Efficiency η_c (percent)
19B-8	Maximum efficiency	14,300	0	24.0	81.7
	Corrected engine speed, 17,500 rpm	17,500	0	29.4	77.6
19XB-1	Maximum efficiency	14,300	Fixed	23.0	81.3
	Maximum corrected engine speed[a]	16,250	Fixed	27.3	77.4

[a]Maximum allowable turbine temperatures limited the 19XB-1 engine to rotational speeds below the rated value of 16,500 rpm.

Pressures

Pressure ratios. - The relations among compressor pressure ratio, corrected air flow, compressor Mach number, and compressor load coefficient have thus far been discussed. Maximum compressor pressure ratios of 3.45 and 4.15 were obtained with the 19B-8 and 19XB-1 engines, respectively (fig. 8(a)). At conditions of maximum compressor efficiency for each engine, the pressure ratio for the 19B-8 compressor was 2.42 (see figs. 11(a) and 8(a)), and the pressure ratio for the 19XB-1 compressor was 3.21 (see figs. 11(b) and 8(a)). The pressure ratio for the 19B-8 compressor with the tail cone in and static test conditions at a corrected engine speed of 17,500 rpm was about 3.18 (fig. 11(b)). With the same simulated flight conditions, the 19XB-1 compressor produced a pressure ratio of 4.15 at a corrected engine speed of 16,250 rpm (fig. 11(b)).

Pressure coefficients. - Compressor pressure coefficients are determined by the compressor characteristics and the position of the engine operating line. Variations of pressure coefficient with

changing flight conditions result from variations in the position of the operating line. Compressor pressure-coefficient contours for the 19B-8 compressor are presented in figure 12. The operating lines from figures 9 and 10 were replotted in figure 12 and the lines of constant average pressure coefficient per stage were obtained from figures 13 to 15. The data available for the 19XB-1 compressor were insufficient to construct this type of curve.

The altitude effect on the compressor pressure coefficient is negligible for both compressors (fig. 13) because the position of the operating line is independent of altitude. Figure 13 also shows that the 19B-8 compressor operated at higher average pressure coefficients per stage than the 19XB-1 compressor. An increase in flight Mach number caused a decrease in compressor pressure coefficient for the 19B-8 compressor (fig. 14). Decreasing the tail-pipe-nozzle area increased the pressure coefficient (fig. 15). An explanation of the effect of tail-cone position on compressor performance has been presented.

The variation of pressure coefficients over the entire range of engine conditions is small. At rated engine speed, the pressure coefficient is slightly less than maximum. The compressor pressure coefficients given in the following table were obtained at static conditions:

Compressor	Conditions	Tail-cone position (in.)	Corrected engine speed $N/\sqrt{\theta}$ (rpm)	Compressor pressure coefficient Ψ
19B-8	Maximum compressor pressure coefficient, Ψ	4	Approx. 13,000	0.312
	Maximum adiabatic temperature-rise efficiency, η_c	0	14,300	.311
	Corrected engine speed $N/\sqrt{\theta}$ of 17,500 rpm	0	17,500	.285
19XB-1	Maximum compressor pressure coefficient, Ψ	Fixed	Approx. 13,400	0.260
	Maximum adiabatic temperature-rise efficiency, η_c	Fixed	14,300	.259
	[a]Maximum corrected engine speed, $N/\sqrt{\theta}$ a	Fixed	16,250	.250

[a]Maximum allowable turbine temperatures limited the 19XB-1 engine to rotational speeds below the rated value of 16,500 rpm.

Compressor-outlet pressure distribution. - Total-pressure distributions across the compressor-outlet annulus for the 19B-8 and 19XB-1 compressors are presented in figures 16 and 17, respectively.

These pressure distributions are cross plots taken from the relation between local compressor pressure ratio and corrected engine speed. The compressor pressure ratio is higher near the blade tip than at the root throughout the entire range of engine speeds for both engines.

Comparison with Dynamometer Data

A comparison of the compressor data obtained from tests of the complete turbojet engine in the altitude wind tunnel at a simulated altitude of 20,000 feet with the performance characteristics of the compressor obtained from dynamometer investigations at a simulated altitude of 22,000 feet (reference 4) is presented in figure 18. When the compressor is an integral part of the 19B-8 turbojet engine, it operates on the low-air-flow side of the maximum-efficiency region (fig. 18). Compressor efficiencies obtained in the altitude wind tunnel and the compressor dynamometer tests are compared in figure 19. The differences in compressor efficiency obtained by the two methods are attributed to the differences in setup.

SUMMARY OF RESULTS

Compressor performance characteristics obtained from results of the altitude-wind-tunnel investigation of the 19B-8 and 19XB-1 turbojet engines are as follows:

1. Variations of altitude (Reynolds number) had no measurable effect on the relations among corrected air flow, compressor Mach number, compressor load coefficient, compressor pressure ratio, and compressor efficiency.

2. The operating lines for the 19B-8 compressor lay on the low-air-flow side of the region of maximum efficiency for the compressor.

3. The 19XB-1 and 19B-8 compressors produced maximum pressure ratios of 4.15 and 3.45, respectively.

4. The 19B-8 compressor operated at somewhat higher average pressure coefficients per stage than did the 19XB-1 compressor; the maximum values were 0.312 and 0.260, respectively.

5. The corrected air flow through the 19B-8 compressor was 29.4 pounds per second at a corrected engine speed of 17,500 rpm. At this engine speed the 19B-8 compressor produced a pressure ratio of 3.18 and had an efficiency of 77.6 percent and an average pressure

coefficient per stage of 0.285. The maximum efficiency of the 19B-8 compressor, which was obtained at a lower corrected engine speed, was 81.7 percent. Maximum allowable turbine temperatures limited the 19XB-1 engine to rotational speeds below the rated value of 16,500 rpm. At the maximum corrected engine speed of 16,250 rpm the corrected air flow through the 19XB-1 compressor was 27.3 pounds per second, the pressure ratio was 4.15, the efficiency was 77.4, and the average pressure coefficient per stage was 0.250. The maximum efficiency of the 19XB-1 compressor, which was obtained at a lower corrected engine speed, was 81.3.

Aircraft Engine Research Laboratory,
National Advisory Committee for Aeronautics,
Cleveland, Ohio.

Robert O. Dietz, Jr.,
Mechanical Engineer.

John K. Kuenzig,
Mechanical Engineer.

Approved: Newell D. Sanders
Newell D. Sanders,
Mechanical Engineer.

Newell D. Sanders for
Abe Silverstein,
Aeronautical Engineer.

hmr

REFERENCES

1. Fleming, William A.: Altitude-Wind-Tunnel Investigation of the Westinghouse 19B-2, 19B-8, and 19XB-1 Jet-Prupulsion Engines. I - Operational Characteristics. NACA MR No. E6E06, Bur. Aero., 1946.

2. Fleming, William A., and Dietz, Robert O., Jr.: Altitude-Wind-Tunnel Investigation of the 19B-2, 19B-8, and 19XB-1 Jet-Propulsion Engines. III - Performance and Windmilling Drag Characteristics. NACA RM No. E7C13, Bur. Aero., 1947.

3. Krebs, Richard P., and Suozzi, Frank L.: Altitude-Wind-Tunnel Investigation of the 19B-2, 19B-8, and 19XB-1 Jet-Propulsion Engines. II - Analysis of Turbine Performance of the 19B-8 Engine. NACA RM No. E7A08, Bur. Aero., 1947.

4. Roepcke, Fay A., Burtt, Jack R., and Medeiros, Arthur A.: Performance of Westinghouse 19B Six-Stage Axial-Flow Compressor. NACA MR No. E5K07, Bur. Aero., 1945.

INDEX OF FIGURES

Figure 9. - Effect of simulated flight Mach number on compressor operating line for 19B-8 turbojet engine. Simulated altitude, 5000 feet; tail cone, 0 inches out.
(a) Relation between compressor pressure ratio and corrected air flow.
(b) Relation between compressor pressure ratio and compressor Mach number.
(c) Relation between compressor pressure ratio and compressor load coefficient.

Figure 10. - Effect of tail-cone position on compressor operating line for 19B-8 turbojet engine. Static conditions; simulated altitude, 5000 feet.
(a) Relation between compressor pressure ratio and corrected air flow.
(b) Relation between compressor pressure ratio and compressor Mach number.
(c) Relation between compressor pressure ratio and compressor load coefficient.

Figure 11. - Relation between compressor efficiency and corrected air flow.
(a) 19B-8 turbojet engine.
(b) 19XB-1 turbojet engine; static test conditions.

Figure 12. - Pressure-coefficient contours for 19B-8 compressor.

Figure 13. - Effect of altitude on relation between compressor pressure coefficient and corrected air flow for 19B-8 and 19XB-1 turbojet engines. Static test conditions; 19B-8 tail cone, 0 inches out.

Figure 14. - Effect of simulated flight Mach number on relation between compressor pressure coefficient and corrected air flow for 19B-8 turbojet engine. Simulated altitude, 5000 feet; tail cone, 0 inches out.

Figure 15. - Effect of tail-cone position on relation between compressor pressure coefficient and corrected air flow for 19B-8 turbojet engine. Static test conditions; simulated altitude, 5000 feet.

Figure 16. - Total-pressure distribution across compressor-outlet annulus for 19B-8 turbojet engine as represented by local compressor pressure ratio.
(a) Static conditions; simulated altitude, 5000 and 20,000 feet; tail cone, 0 inches out.
(b) Simulated flight Mach number, 0.312; simulated altitude, 5000 feet; tail cone, 0 inches out.
(c) Static conditions; simulated altitude, 5000 feet; tail cone, 4 inches out.

Figure 17. - Total-pressure distribution across compressor-outlet annulus for 19XB-1 turbojet engine as represented by local compressor pressure ratio. Static conditions; simulated altitudes, 5000, 20,000, and 25,000 feet.

Figure 18. - Comparison of data for 19B compressor obtained in altitude-wind-tunnel investigation of complete engine at static conditions with tail cone in with data obtained in dynamometer tests (reference 4).

Figure 19. - Comparison of compressor efficiencies for 19B-8 compressor obtained in altitude-wind-tunnel investigation of complete engine with efficiencies obtained in dynamometer tests.

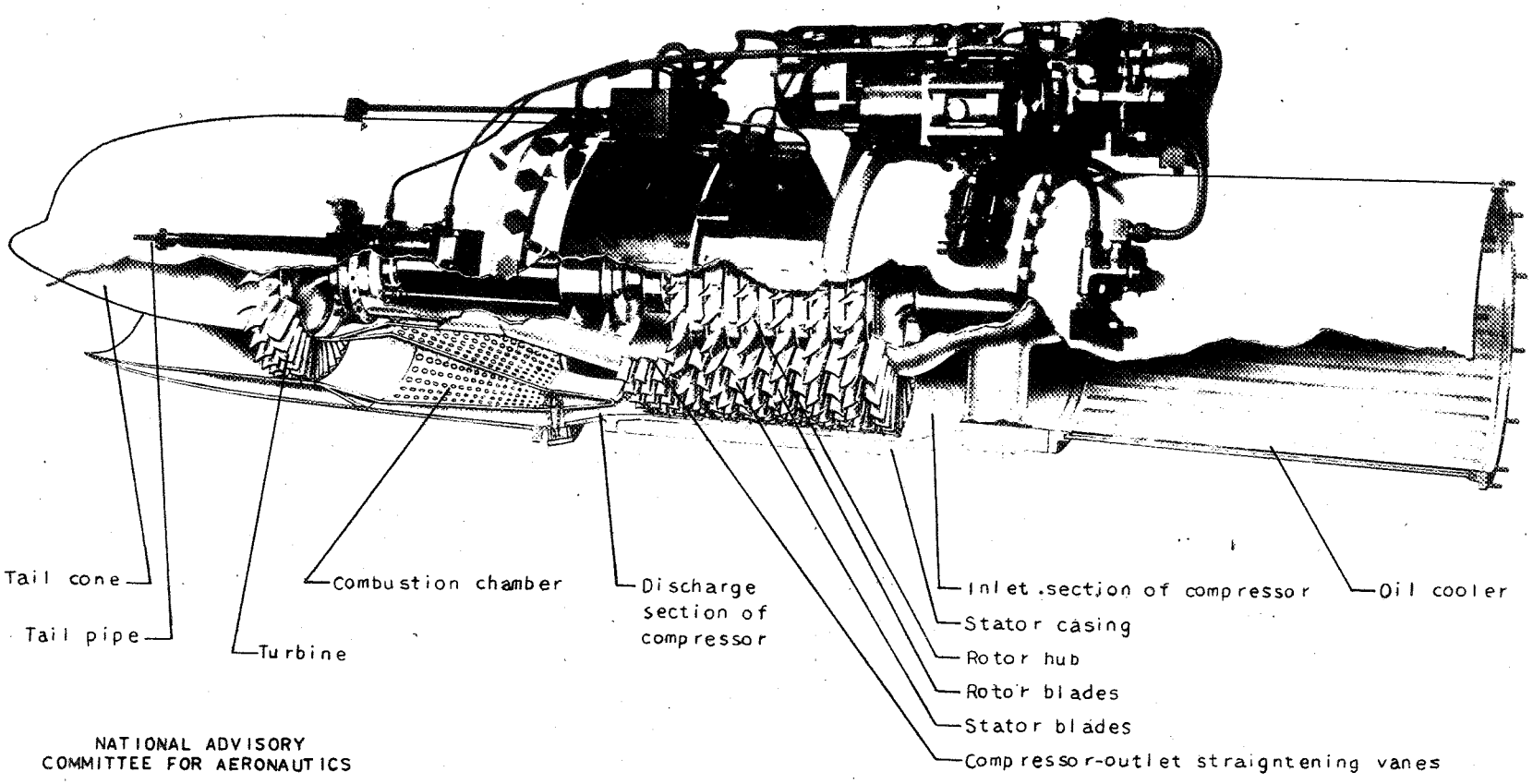

Figure 1. - Compressor installation in 19B turbojet engine.

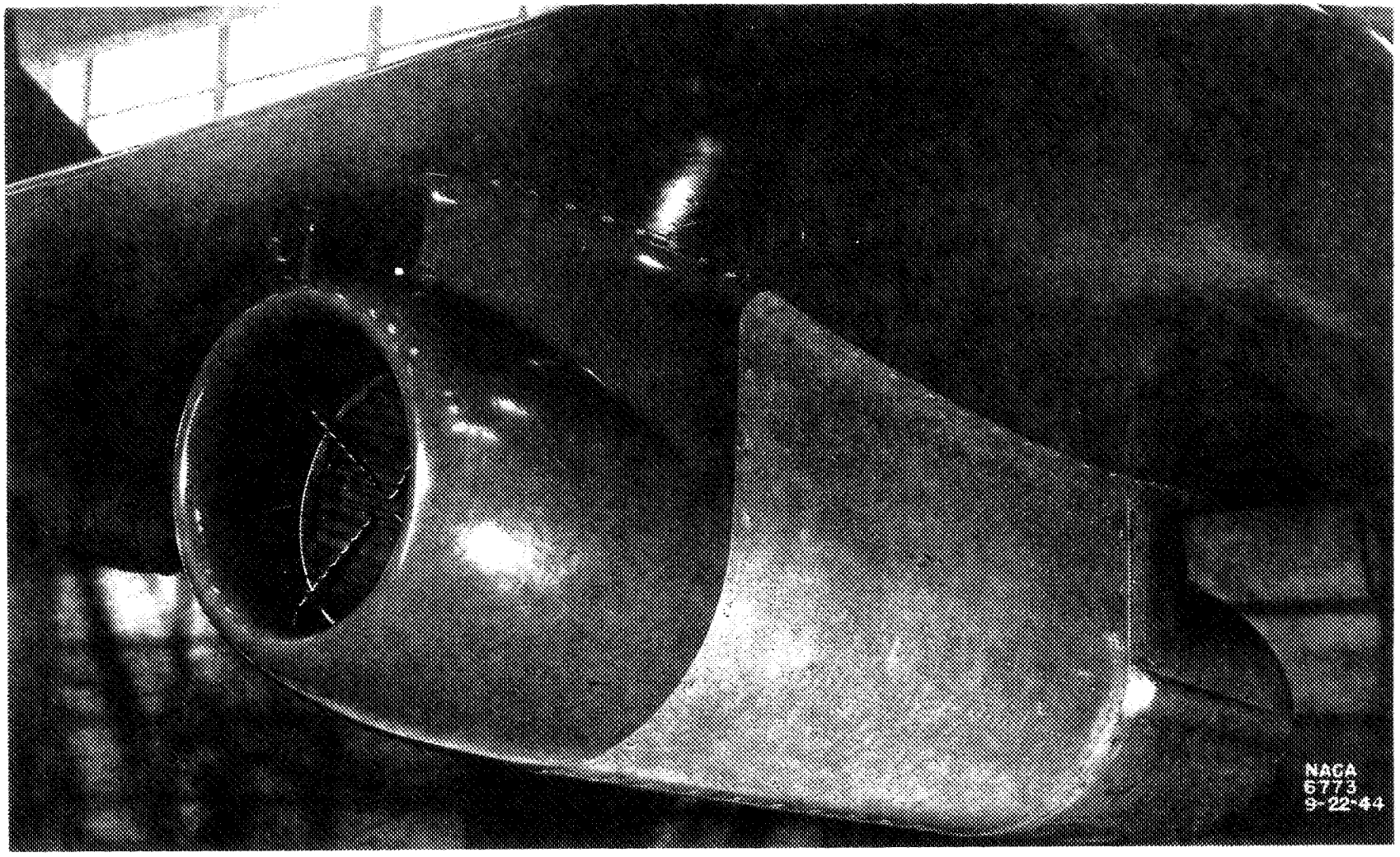

(a) Left-side view with cowling installed.

Figure 2. - Installation of I98 turbojet engine in wing nacelle for investigation in altitude wind tunnel.

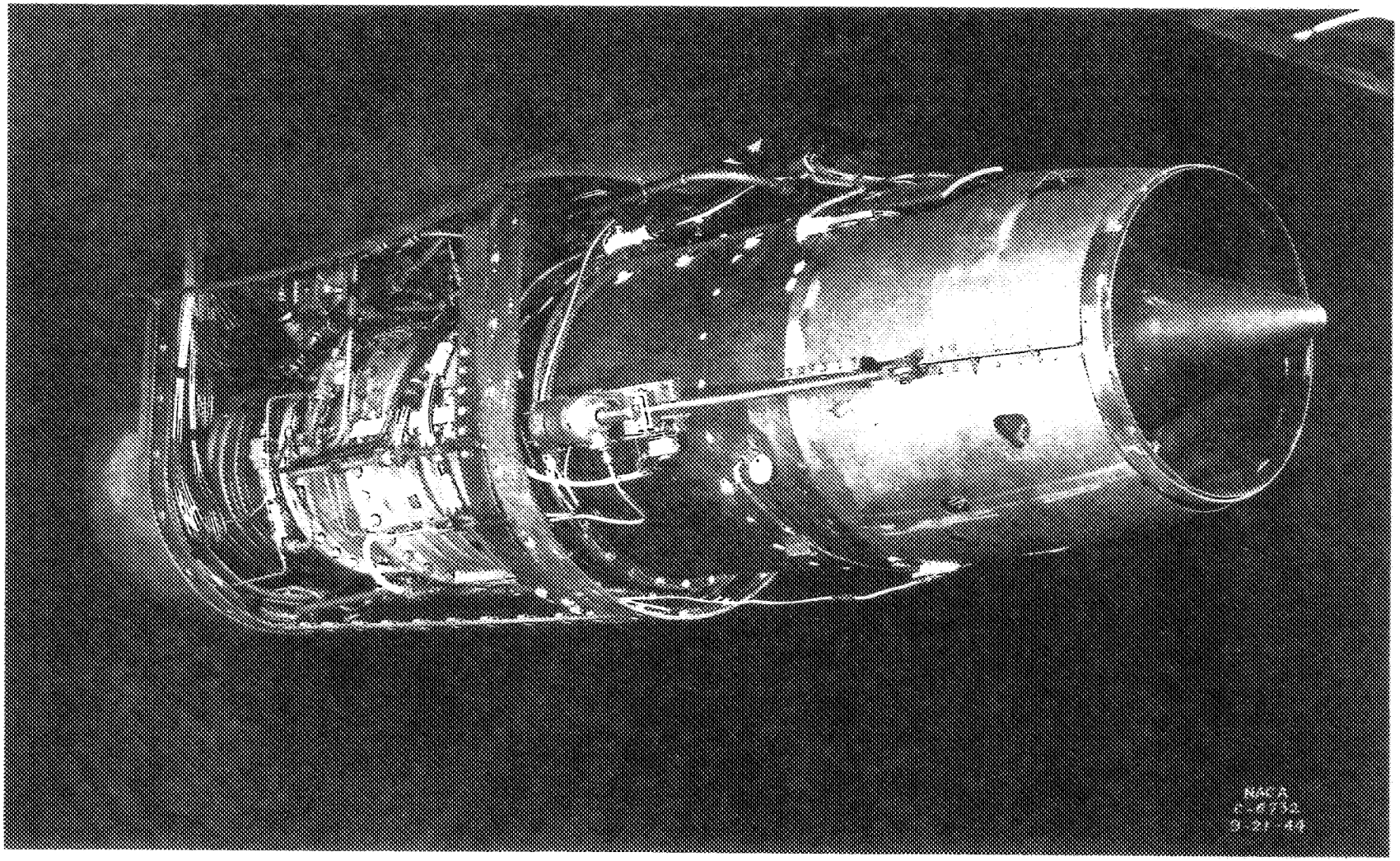

(b) Left-side view with cowling removed.

Figure 2. - Continued. Installation of 19B turbojet engine in wing nacelle for investigation in altitude wind tunnel.

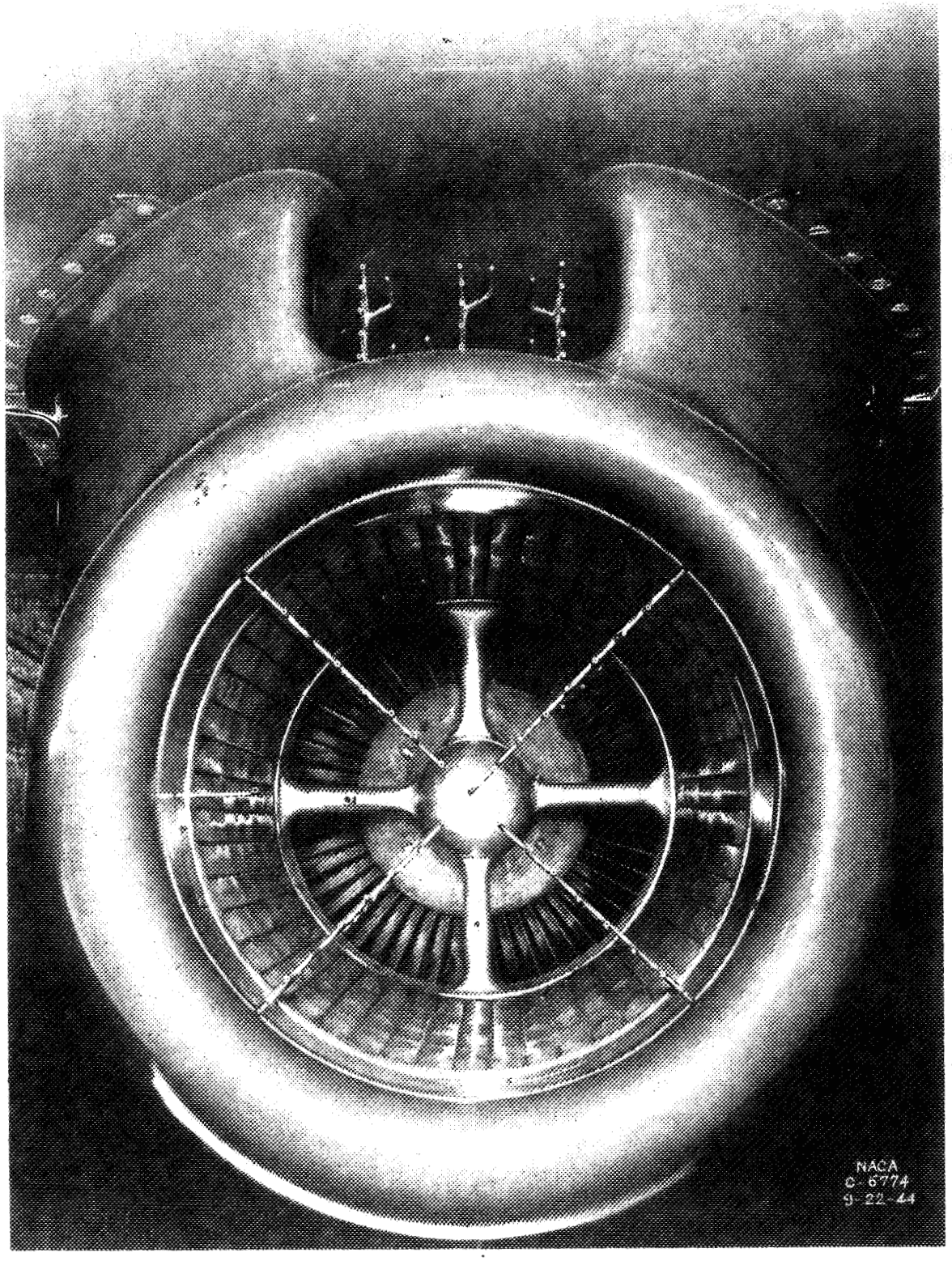

(c) Front view with inlet screen removed.

Figure 2. - Concluded. Installation of 19B turbojet engine in wing nacelle for investigation in altitude wind tunnel.

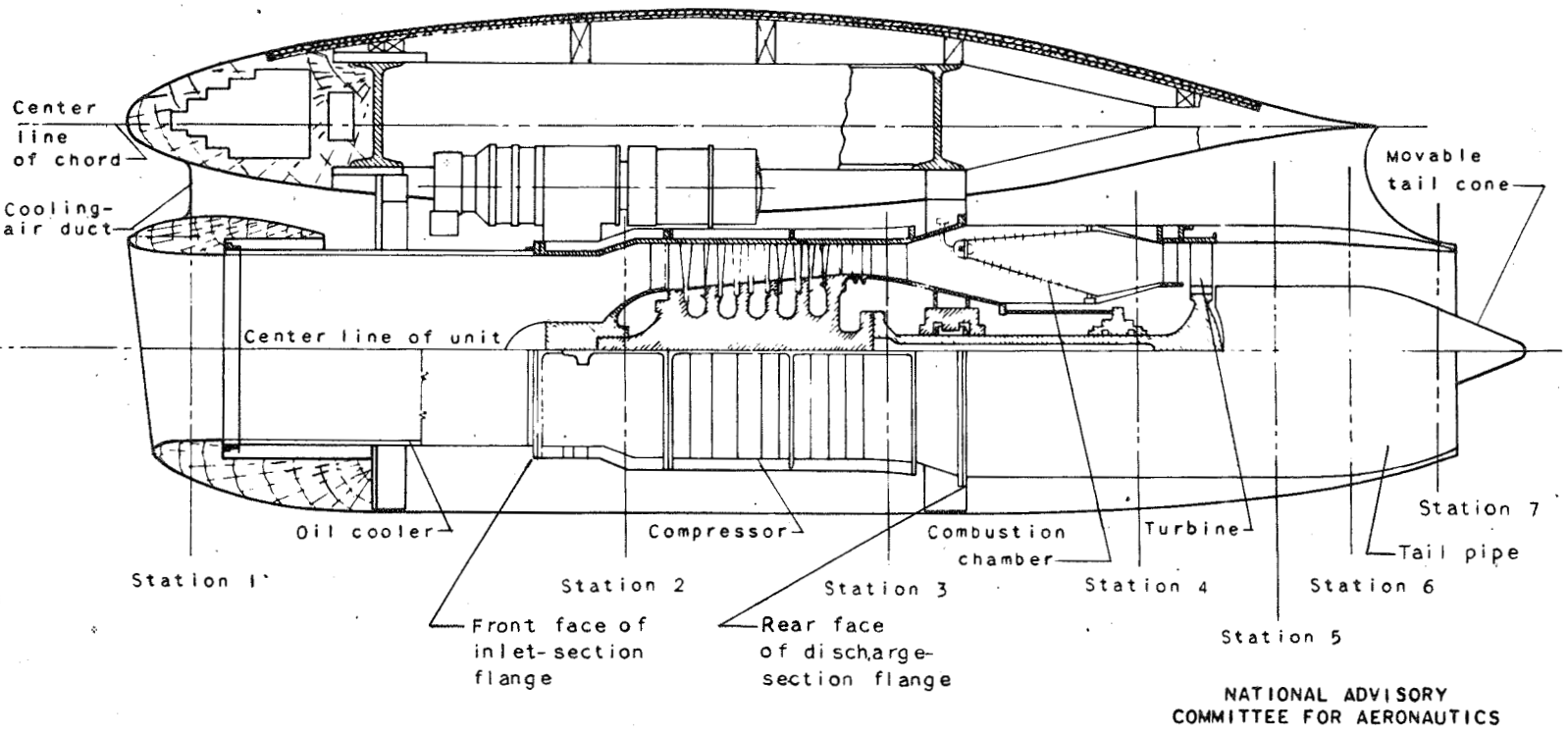

Figure 3. - Longitudinal section of 19B turbojet-engine installation showing measuring stations.

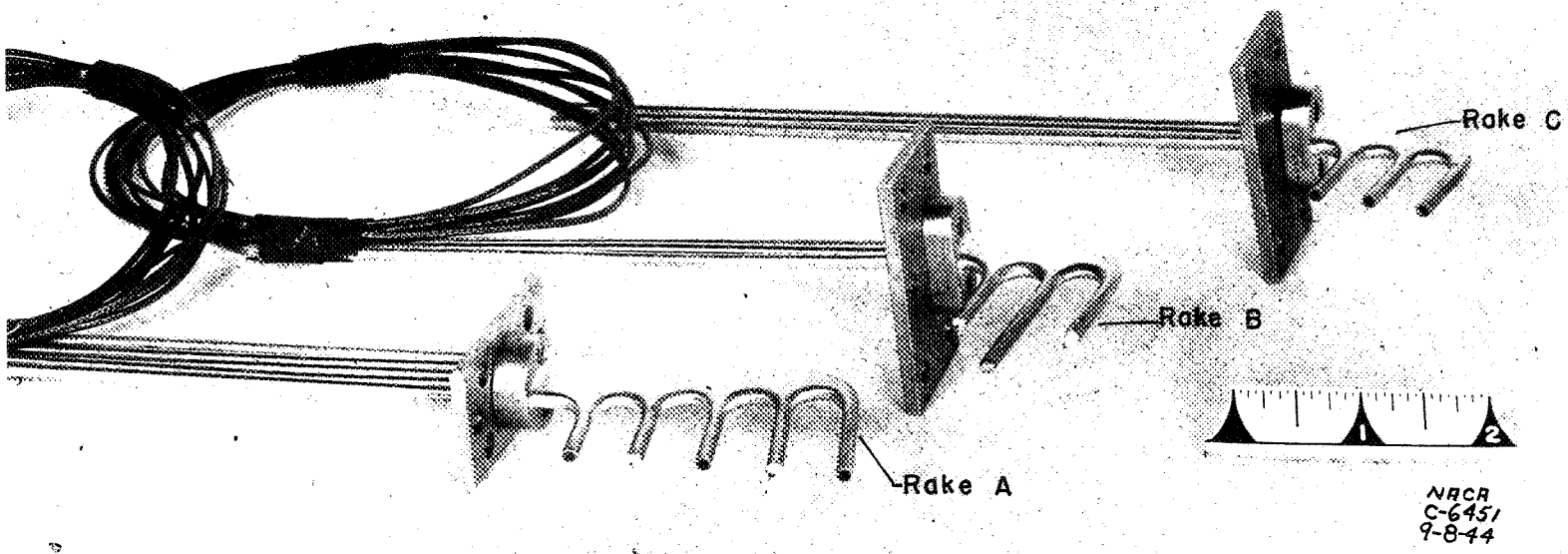

Figure 4. - Inconel pressure and temperature rakes installed in compressor inlet (station 2) $3\frac{1}{8}$ inches upstream of front flange of split stator casing and in compressor outlet (station 3) $1\frac{31}{32}$ inches upstream of rear flange of split stator casing.

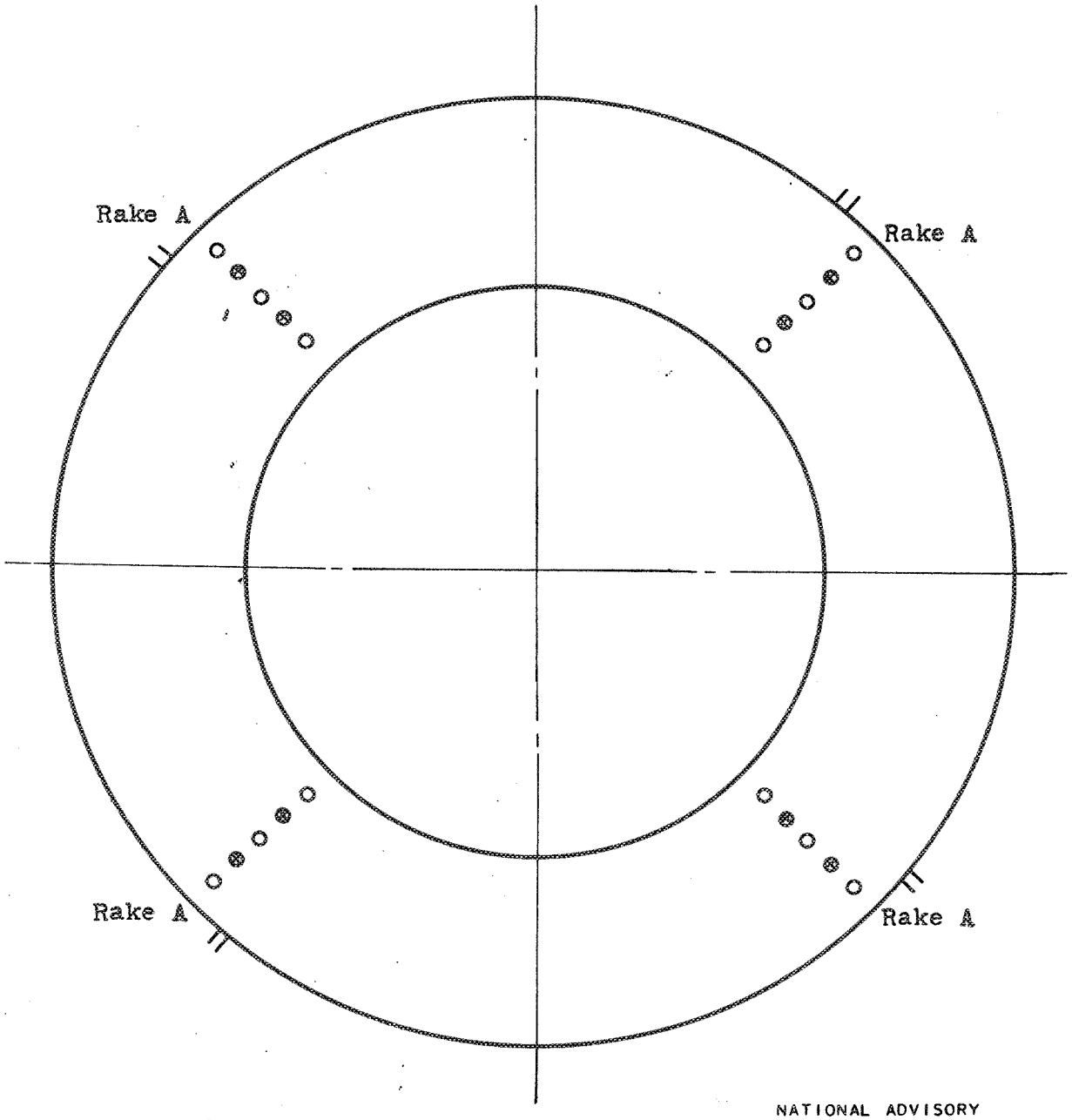

Figure 5.- Location of survey instrumentation at compressor inlet (station 2) for 19B-8 and 19XB-1 turbojet engines.

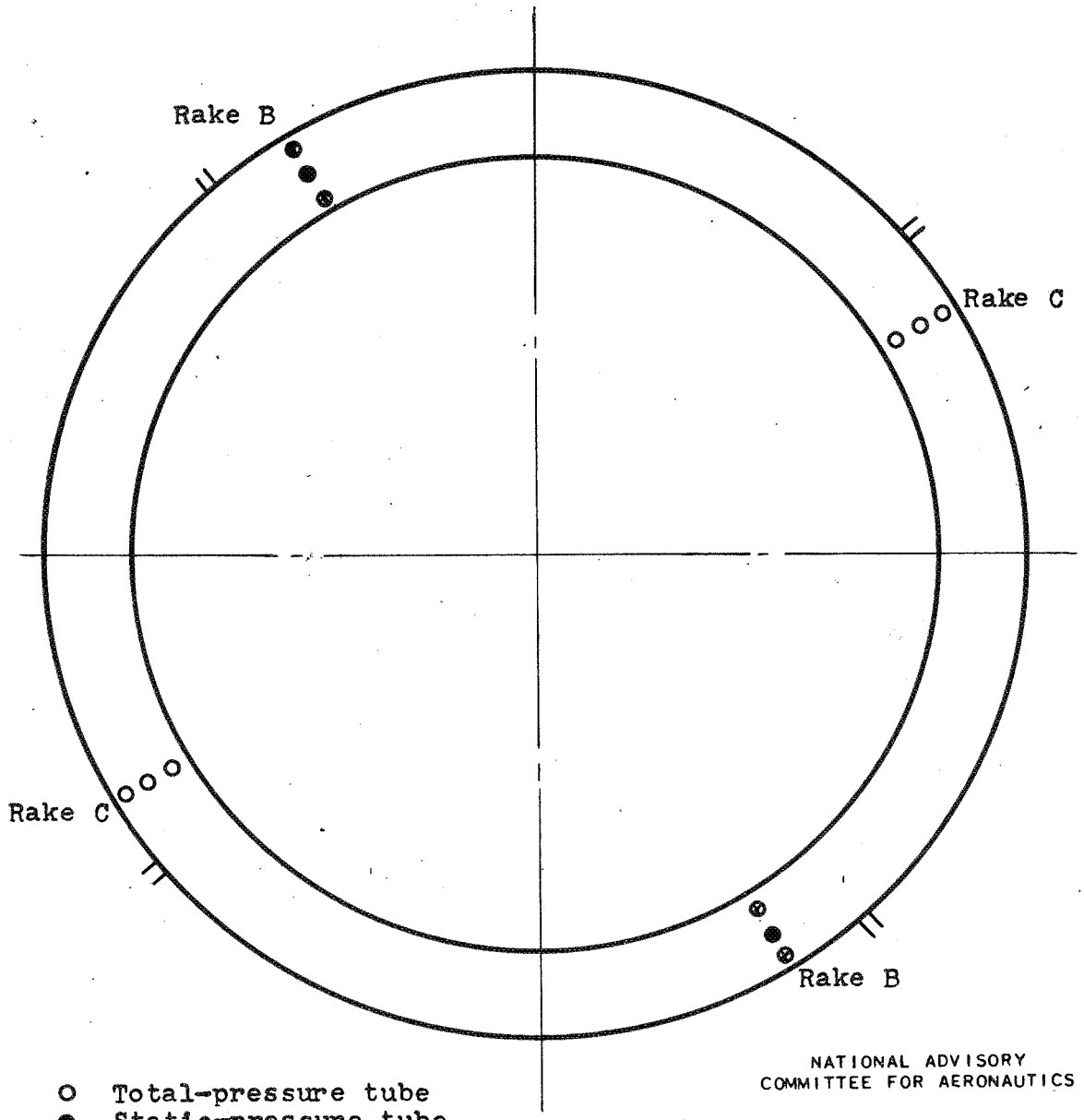

(a) 19B-8 turbojet engine.

Figure 6.- Location of survey instrumentation at compressor outlet (station 3).

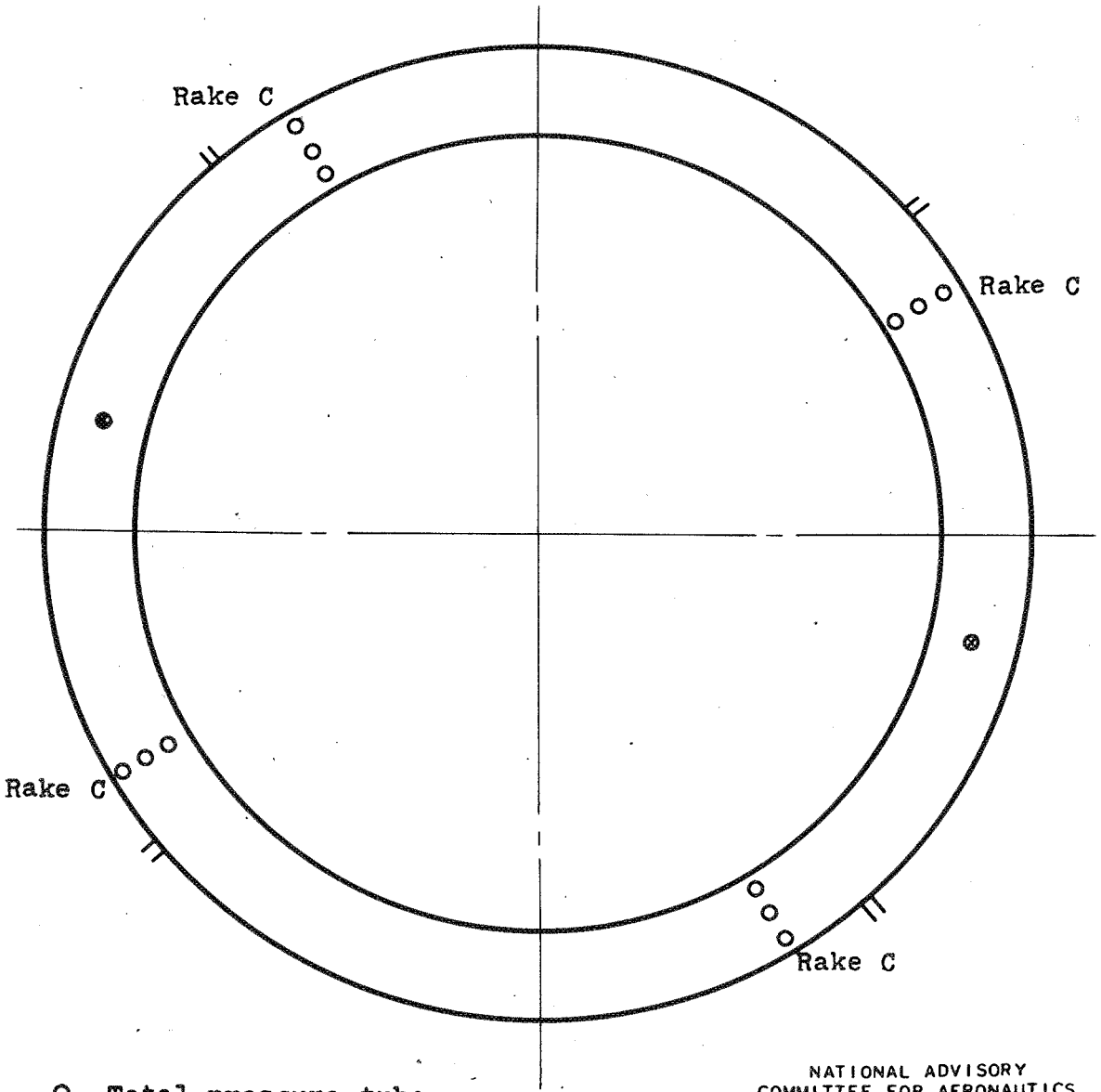

(b) 19XB-1 turbojet engine.

Figure 6.- Concluded. Location of survey instrumentation at compressor outlet (station 3).

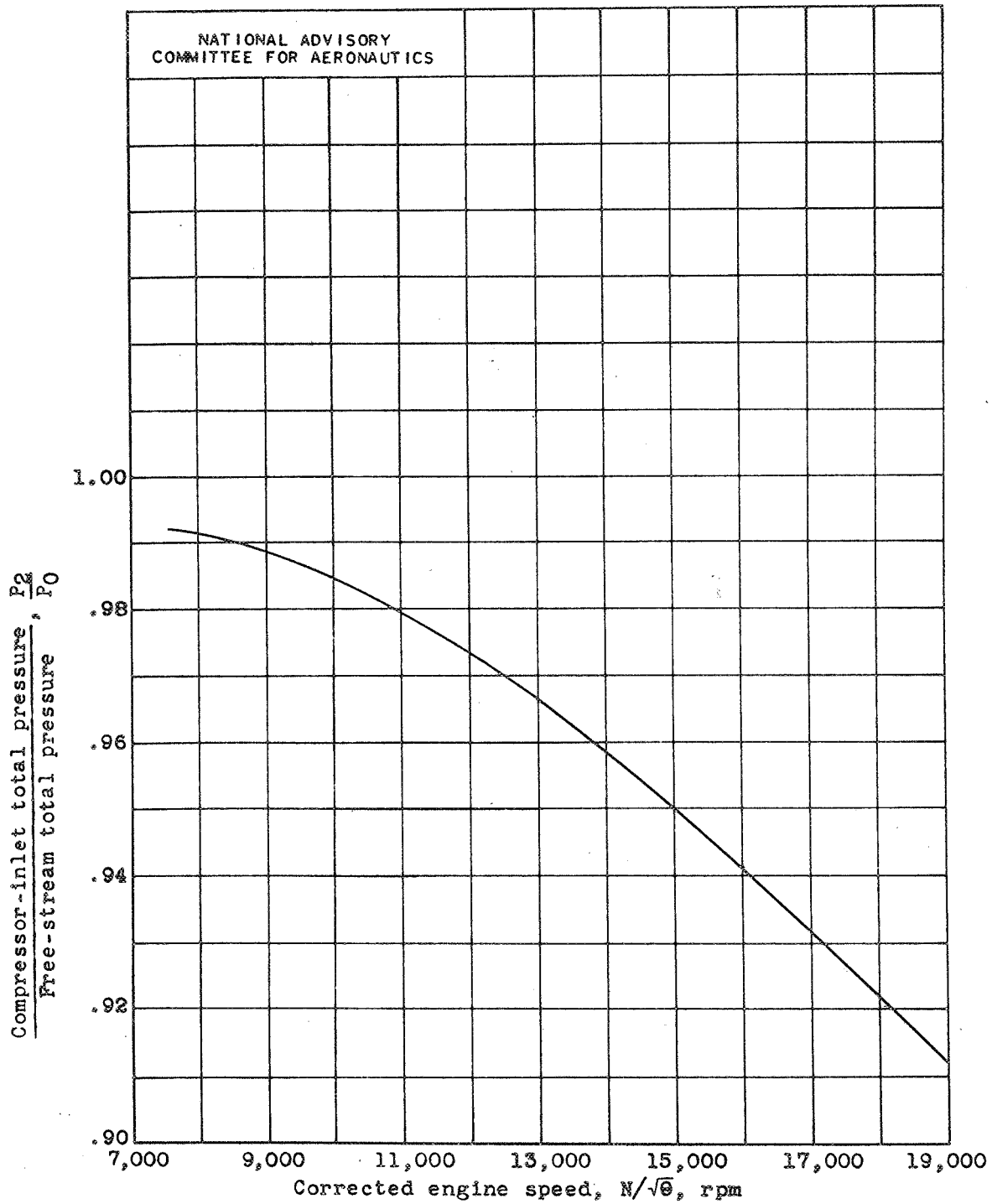

Figure 7.- Relation between total-pressure ratio across cowl-inlet screen and corrected engine speed. Flight Mach number, 0.03 to 0.317; simulated altitude, 0 to 25,000 feet.

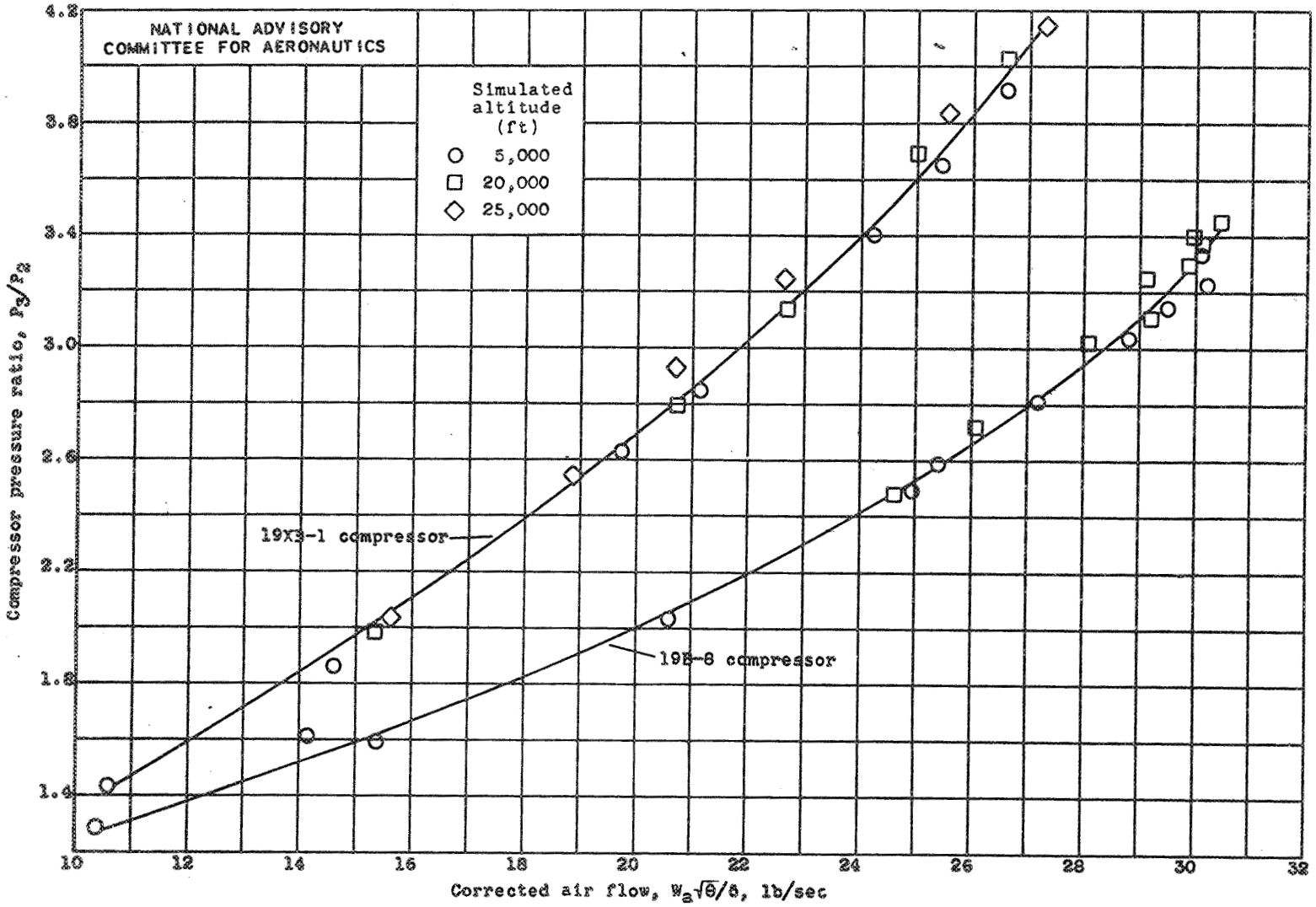

(a) Relation between compressor pressure ratio and corrected air flow.

Figure 8.- Effect of simulated altitude on compressor operating line for 19B-8 and 19XB-1 turbojet engines. Static conditions; 19B-8 tail cone, 0 inches out.

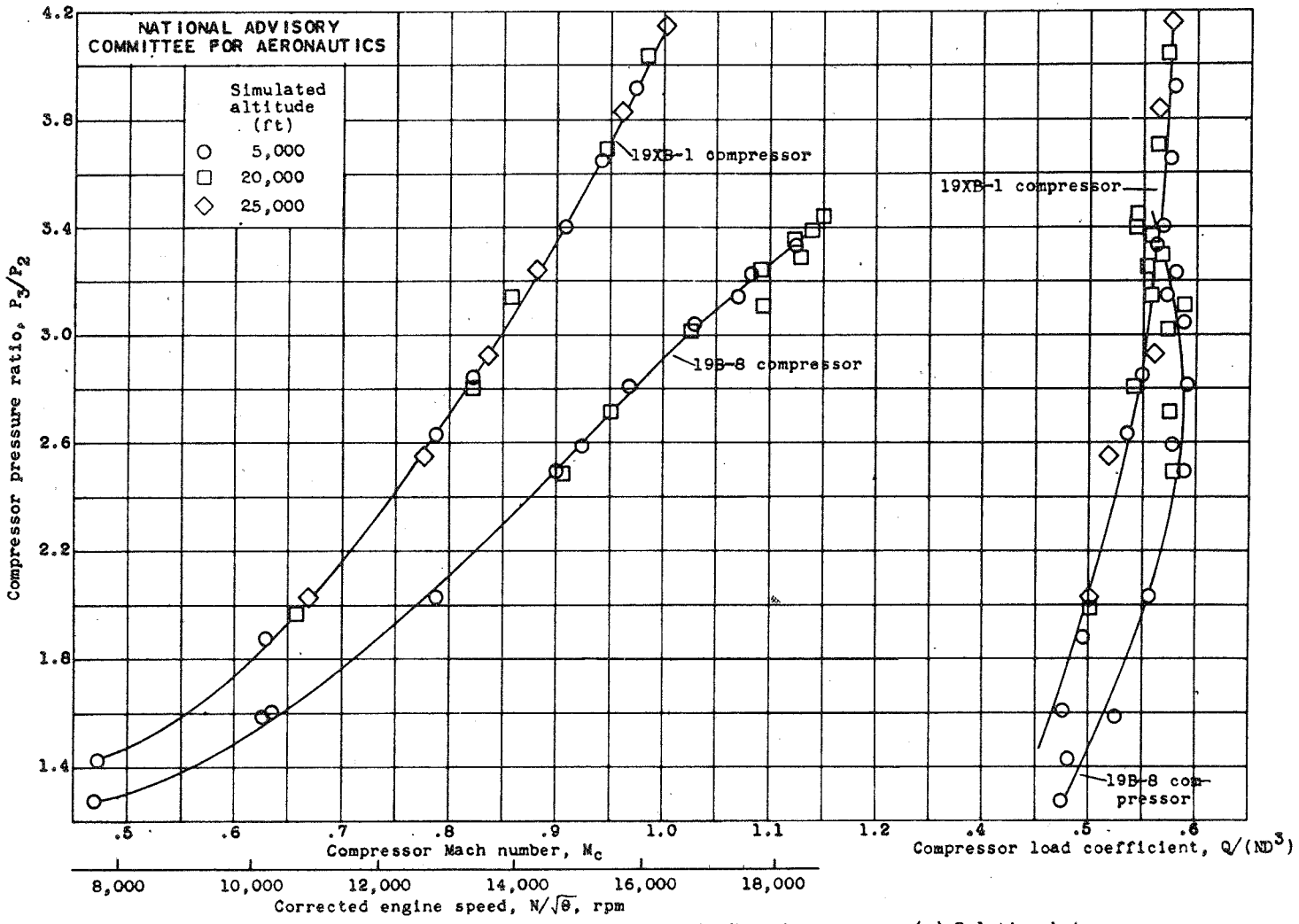

(b) Relation between compressor pressure ratio and compressor Mach number.

(c) Relation between compressor pressure ratio and compressor load coefficient.

Figure 8.- Concluded. Effect of simulated altitude on compressor operating line for 19B-8 and 19XB-1 turbojet engines. Static conditions; 19B-8 tail cone, 0 inches out.

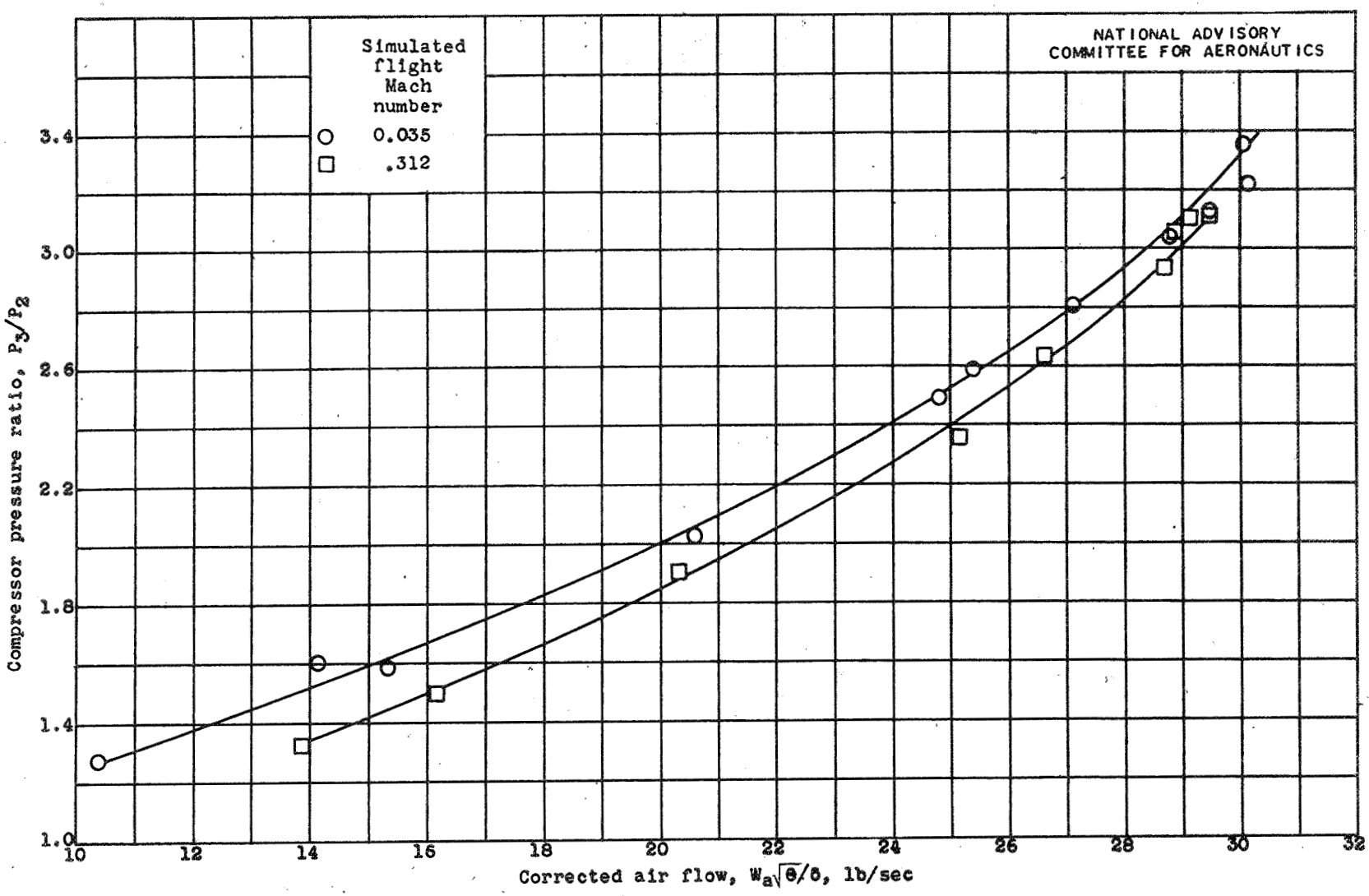

(a) Relation between compressor pressure ratio and corrected air flow.

Figure 9.- Effect of simulated flight Mach number on compressor operating line for 19B-8 turbojet engine. Simulated altitude, 5000 feet; tail cone, 0 inches out.

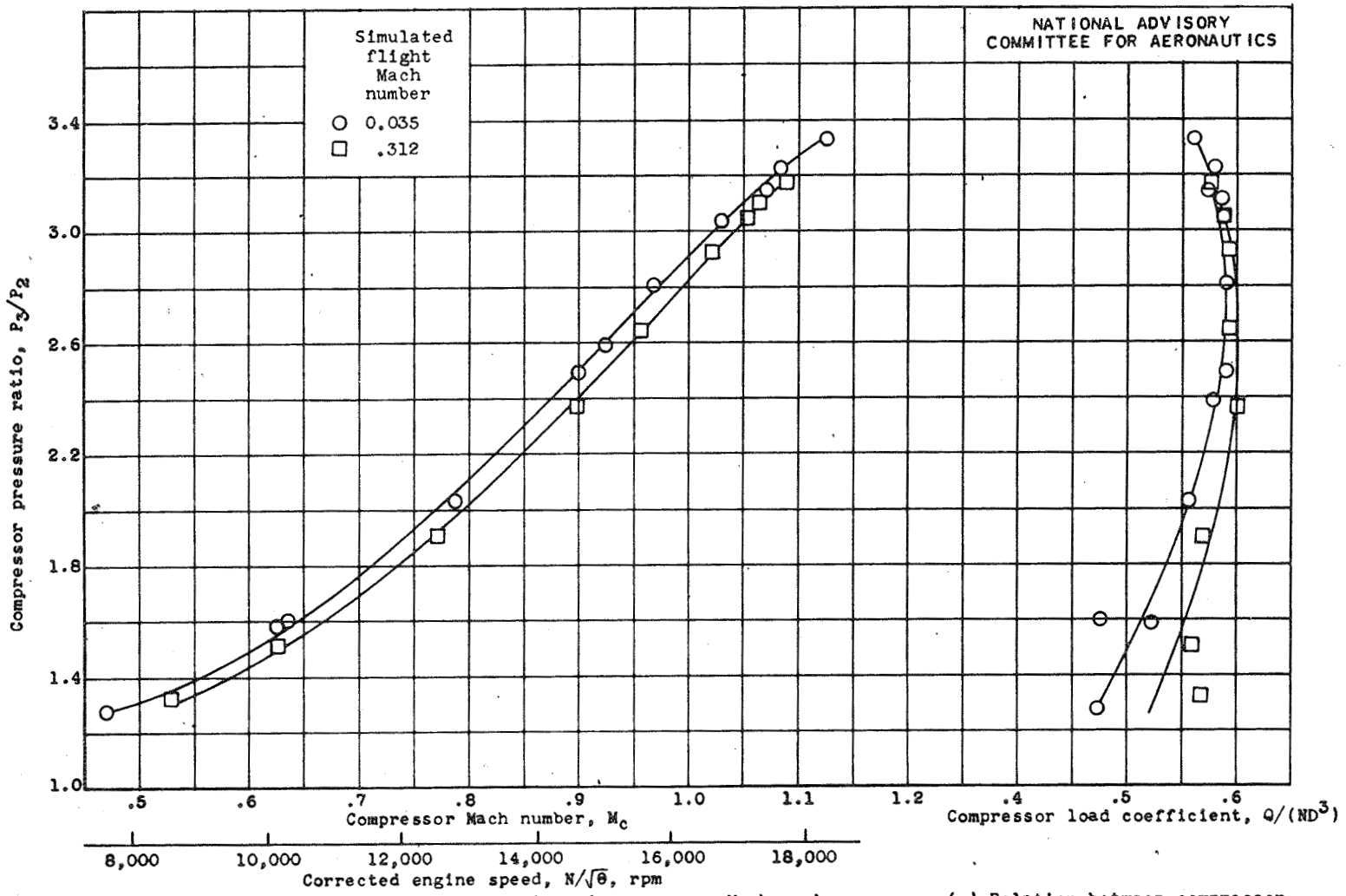

(b) Relation between compressor pressure ratio and compressor Mach number.

(c) Relation between compressor pressure ratio and compressor load coefficient.

Figure 9.- Concluded. Effect of simulated flight Mach number on compressor operating line for 19B-8 turbojet engine. Simulated altitude, 5000 feet; tail cone, 0 inches out.

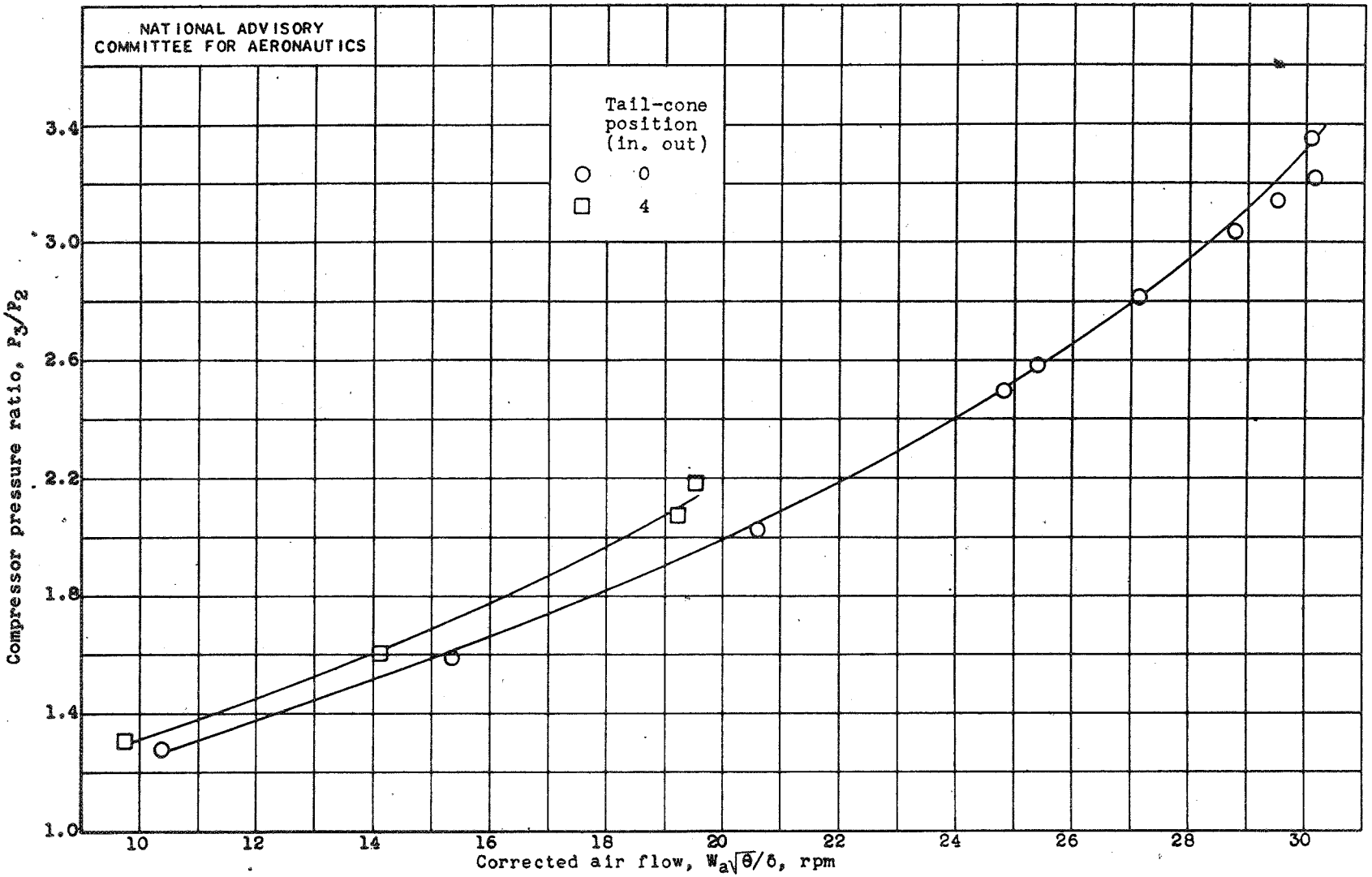

(a) Relation between compressor pressure ratio and corrected air flow.

Figure 10.- Effect of tail-cone position on compressor operating line for 19B-8 turbojet engine. Static conditions; simulated altitude, 5000 feet.

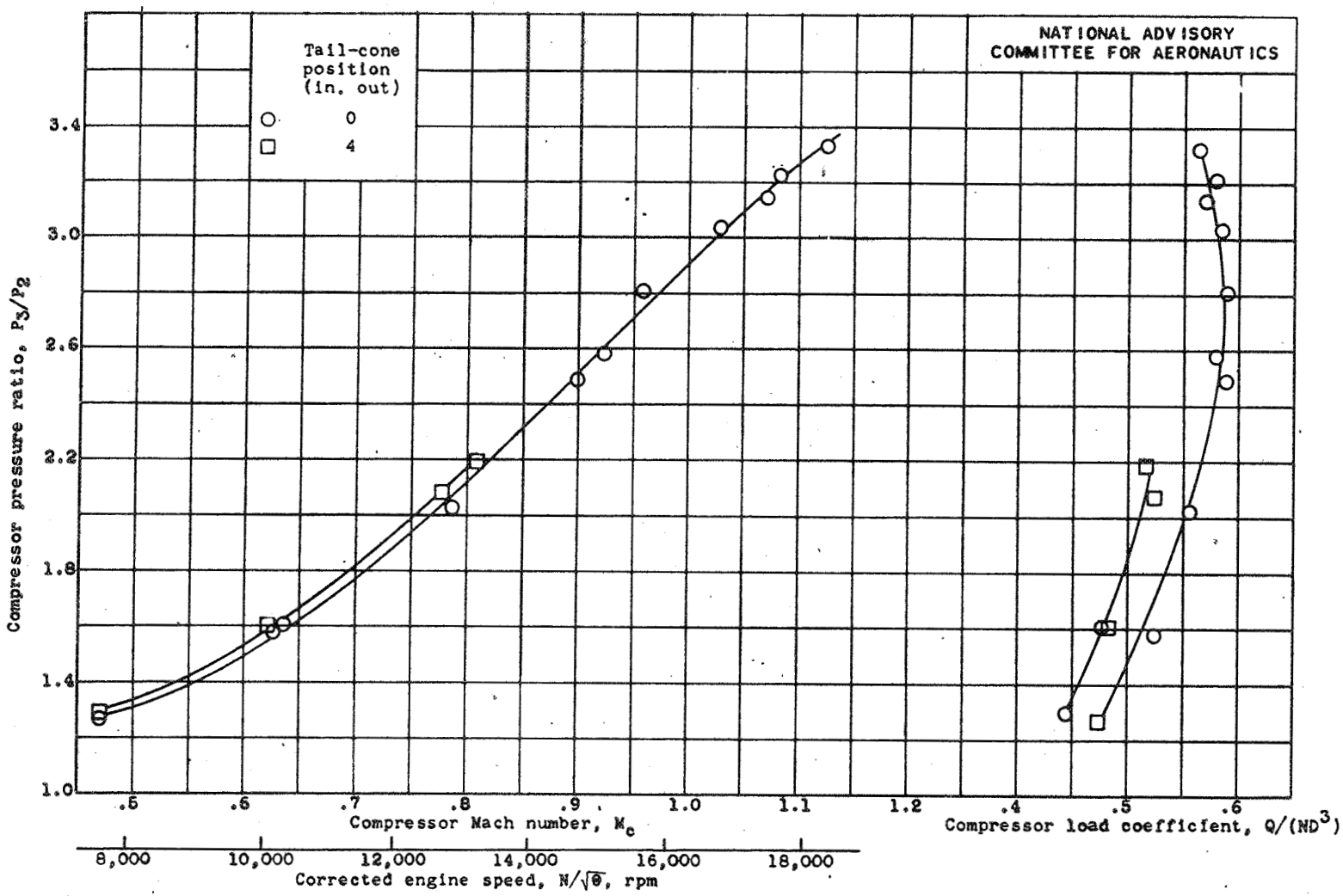

(b) Relation between compressor pressure ratio and compressor Mach number.

(c) Relation between compressor pressure ratio and compressor load coefficient.

Figure 10.- Concluded. Effect of tail-cone position on compressor operating line for 19B-8 turbojet engine. Static conditions; simulated altitude, 5000 feet.

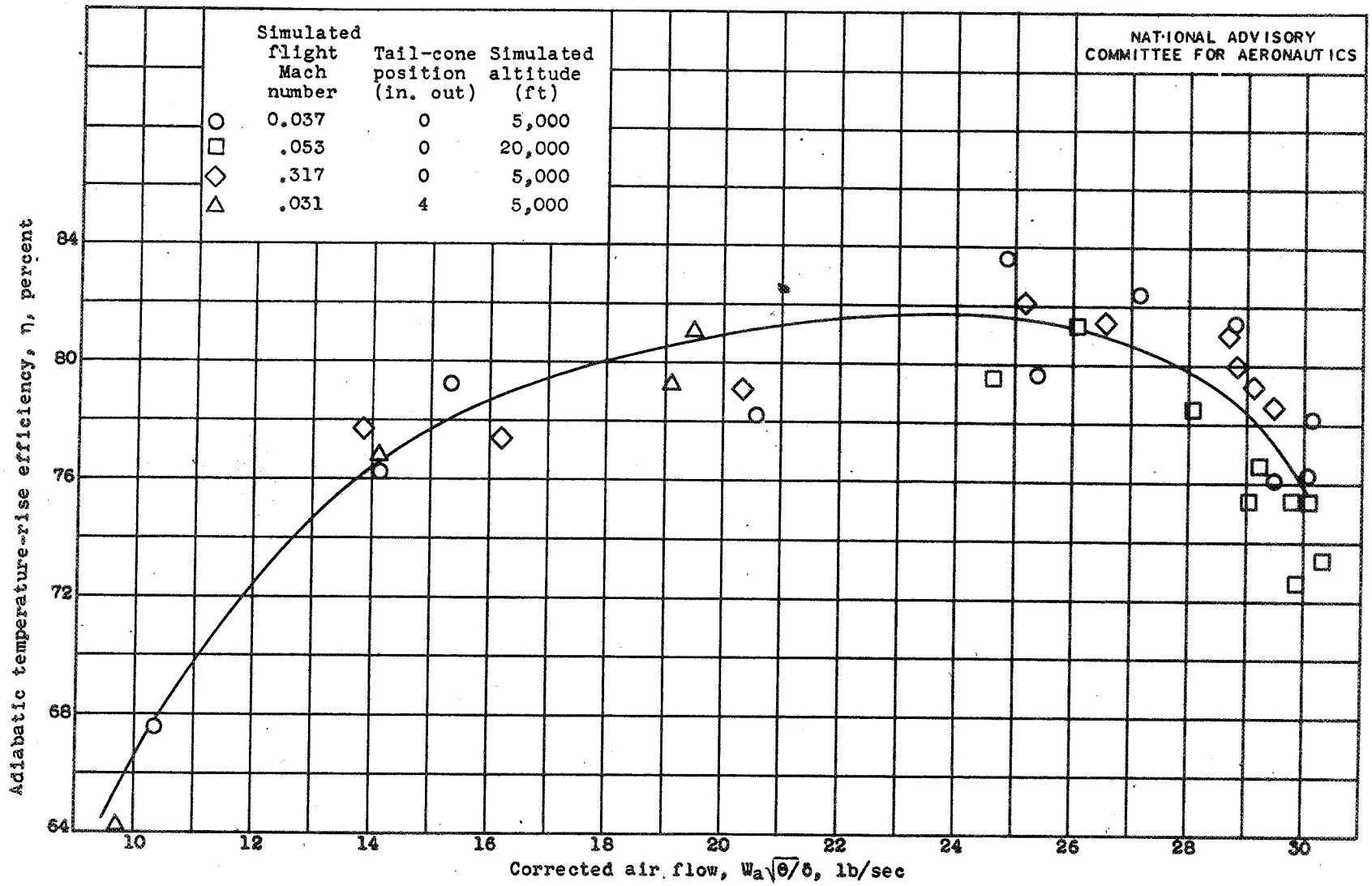

(a) 19B-8 turbojet engine.

Figure 11.- Relation between compressor efficiency and corrected air flow.

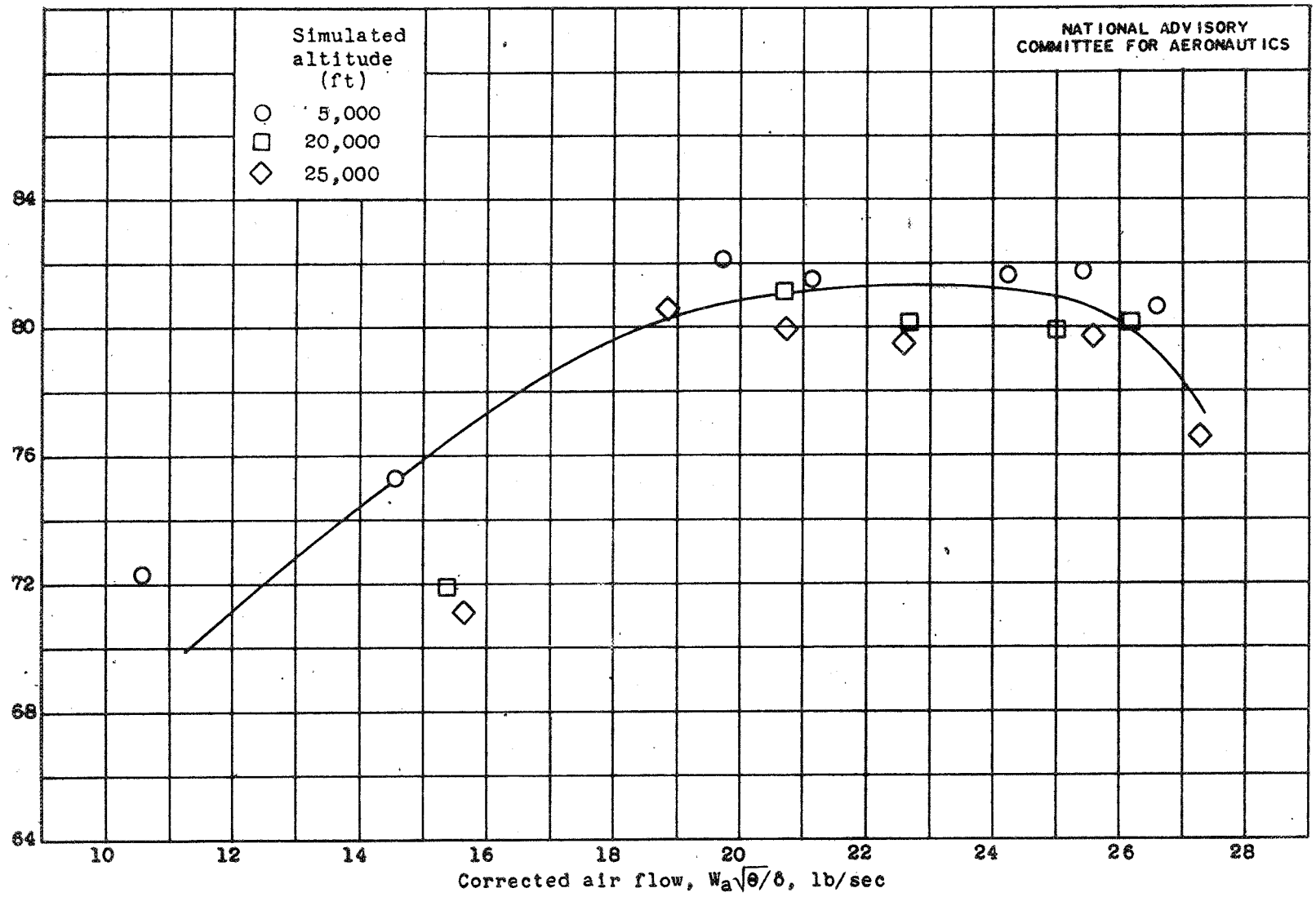

(b) 19XB-1 turbojet engine; static test conditions.

Figure 11.- Concluded. Relation between compressor efficiency and corrected air flow.

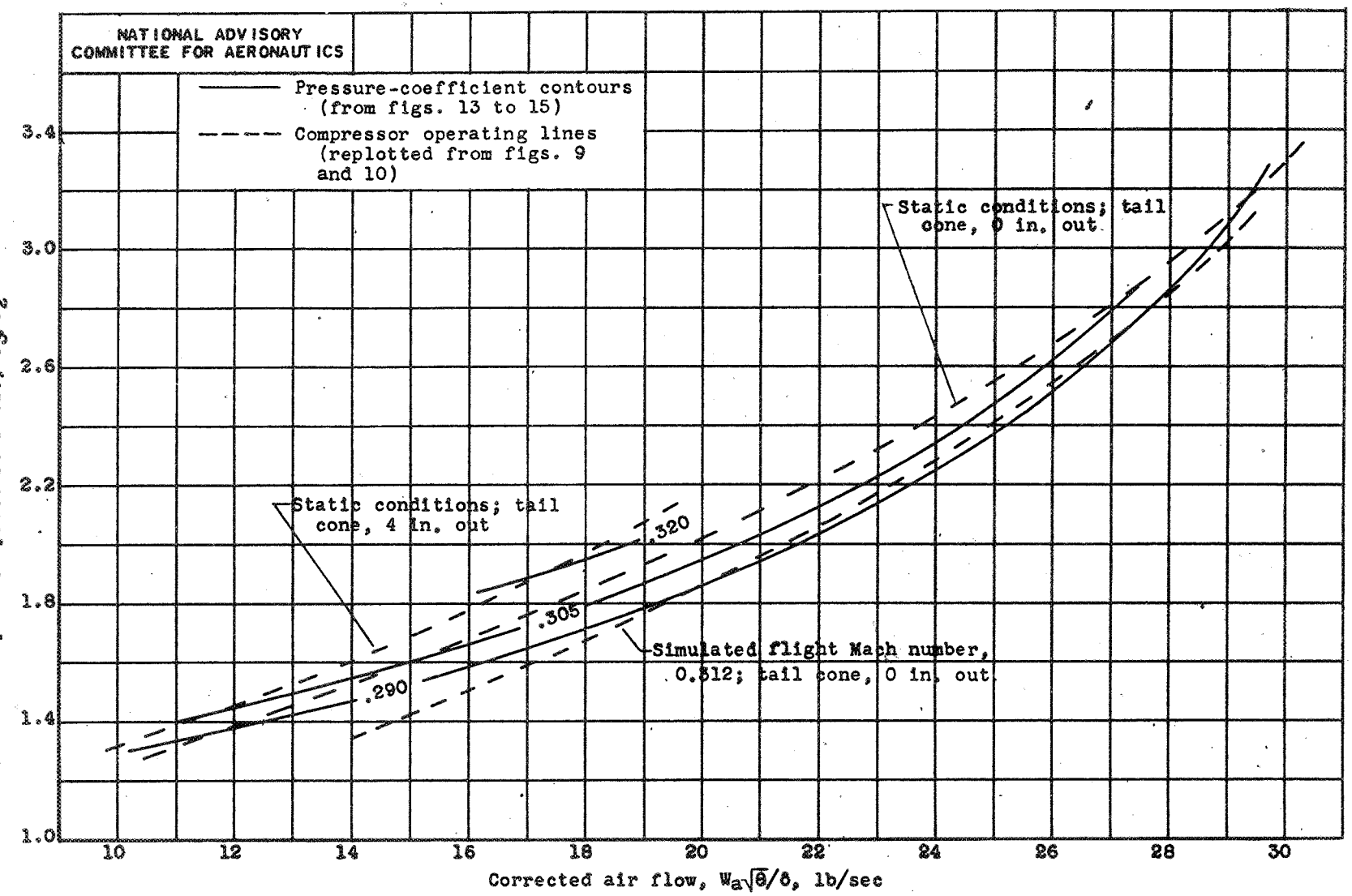

Figure 12.- Pressure-coefficient contours for 19B-8 compressor.

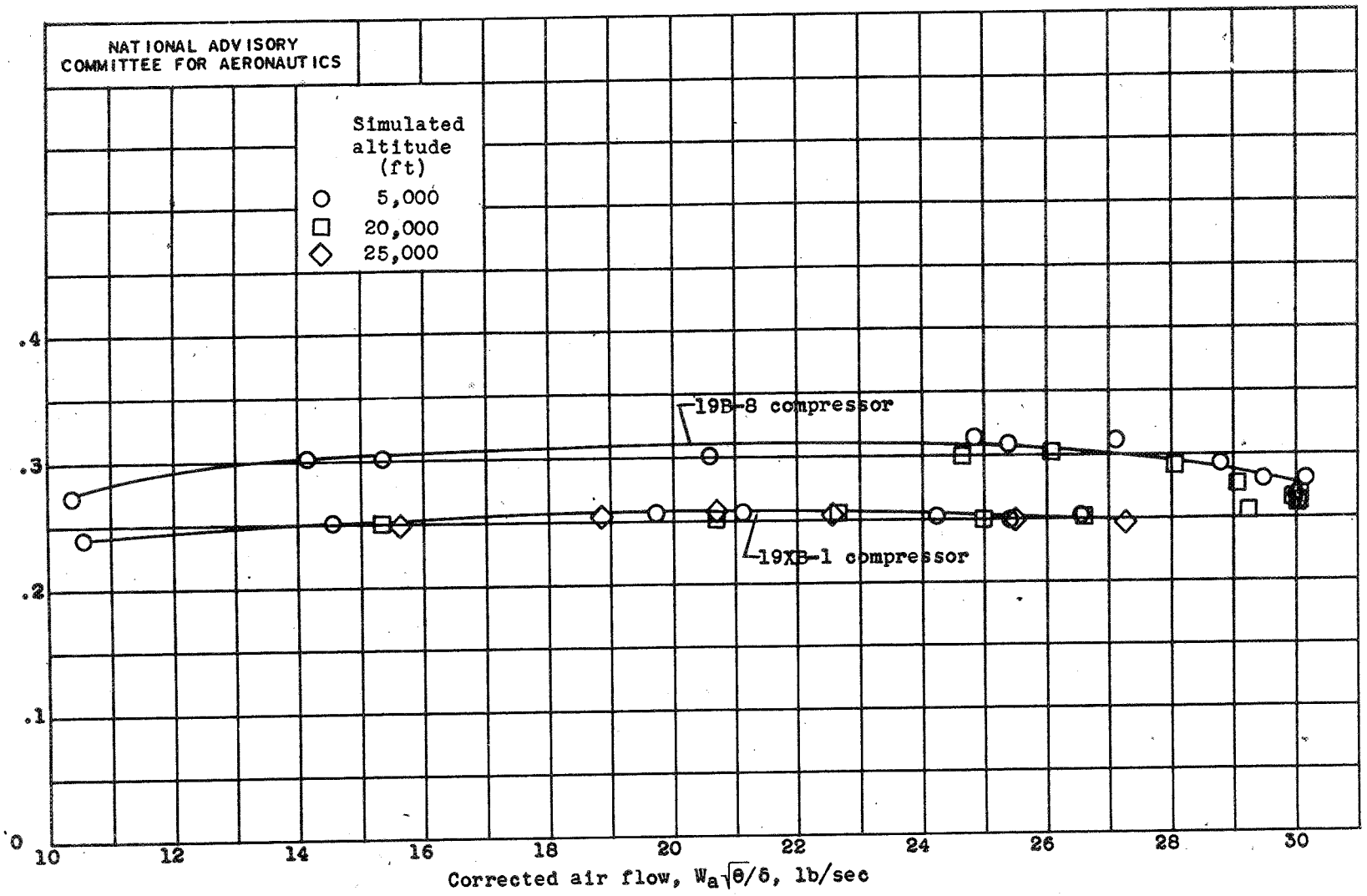

Figure 13.- Effect of altitude on relation between compressor pressure coefficient and corrected air flow for 19B-8 and 19XB-1 turbojet engines. Static test conditions; 19B-8 tail cone, 0 inches out.

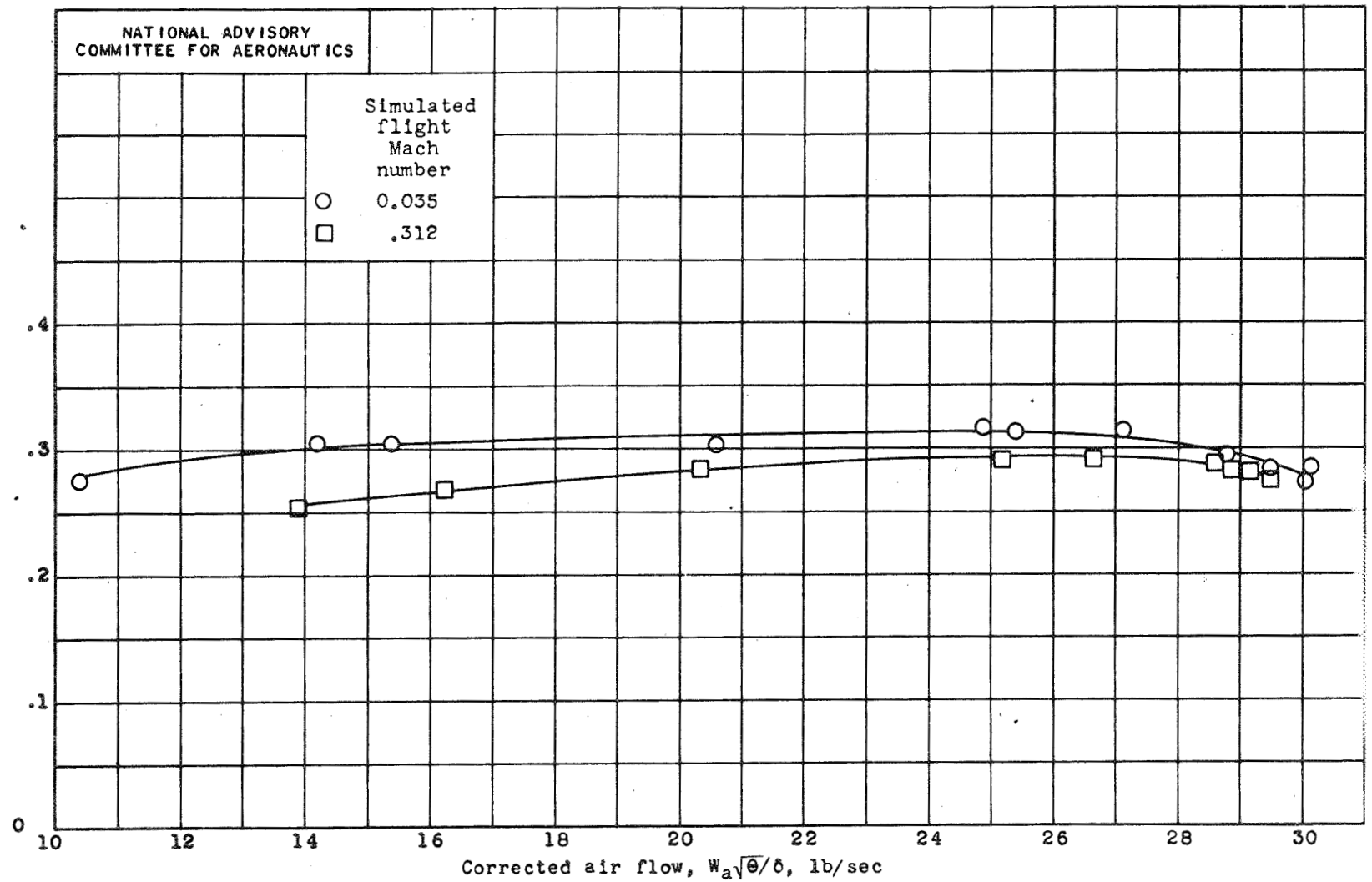

Figure 14.- Effect of simulated flight Mach number on relation between compressor pressure coefficient and corrected air flow for 19B-8 turbojet engine. Simulated altitude, 5000 feet; tail cone, 0 inches out.

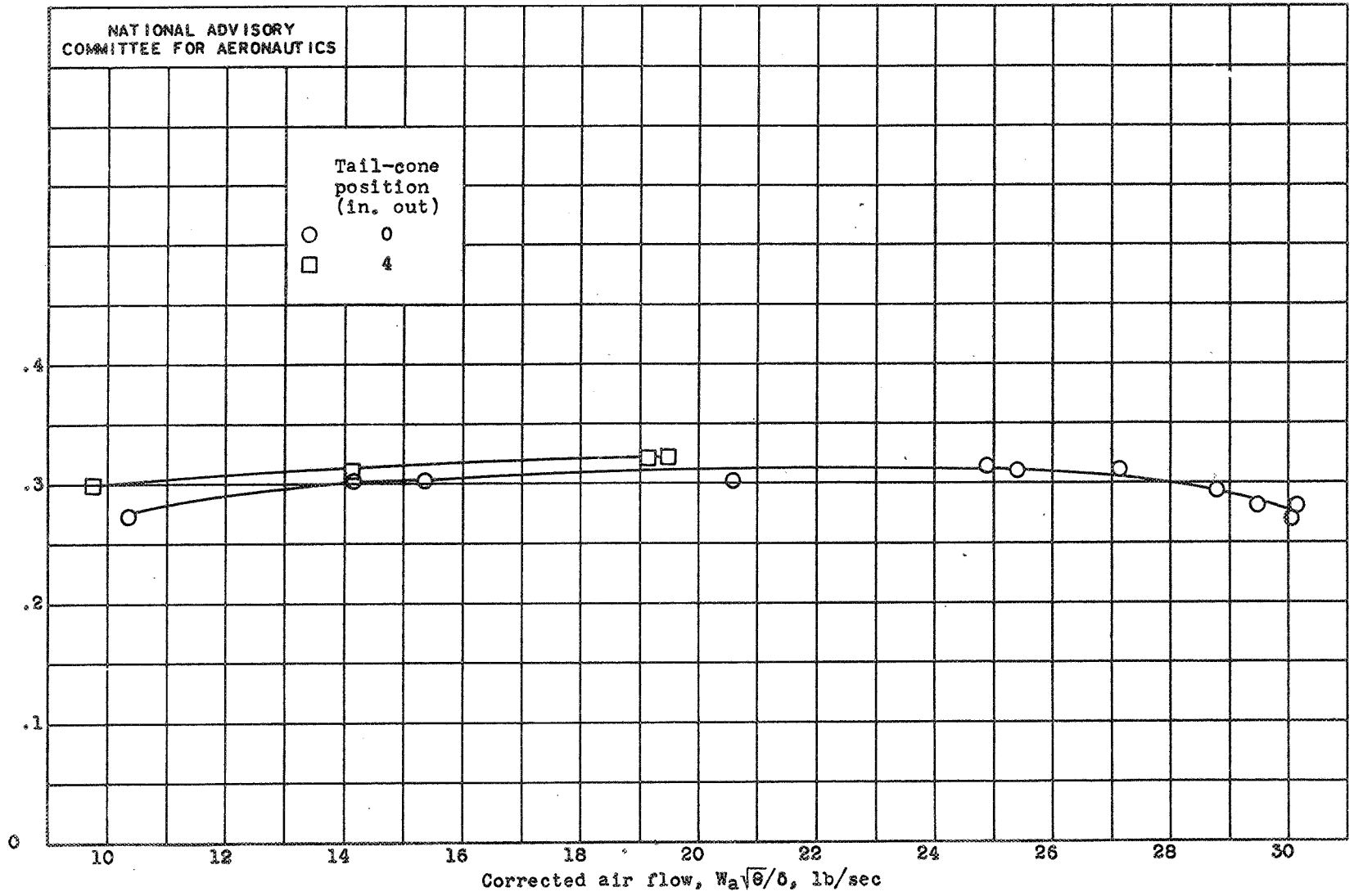

Figure 15.- Effect of tail-cone position on relation between compressor pressure coefficient and corrected air flow for 19B-8 turbojet engine. Static test conditions; simulated altitude, 5000 feet.

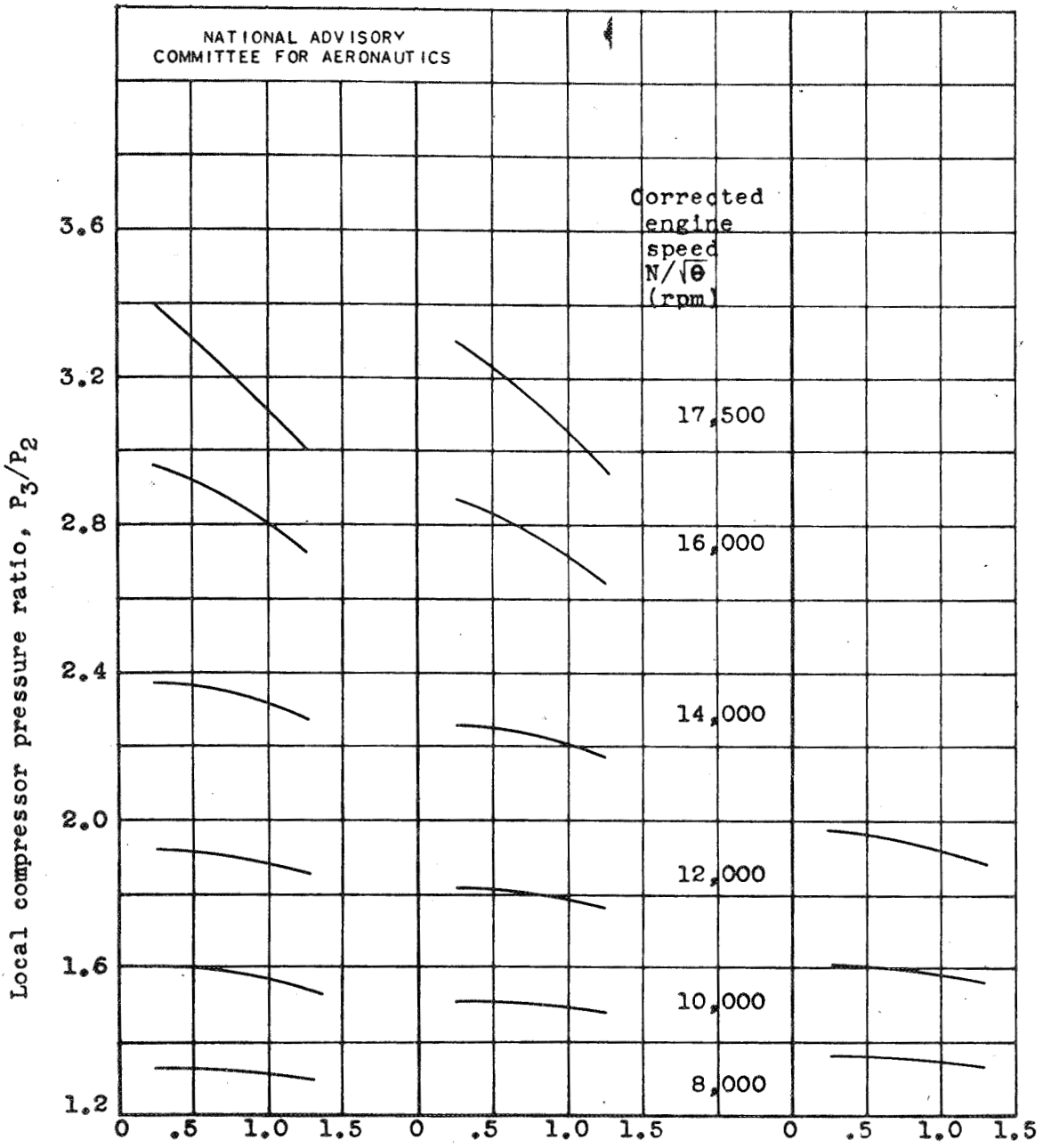

(a) Static conditions; simulated altitude, 5000 and 20,000 feet; tail cone, 0 inches out.

(b) Simulated flight Mach number, 0.312; simulated altitude, 5000 feet; tail cone, 0 inches out.

(c) Static conditions; simulated altitude, 5000 feet; tail cone, 4 inches out.

Figure 16.- Total-pressure distribution across compressor-outlet annulus for 19B-8 turbojet engine as represented by local compressor pressure ratio.

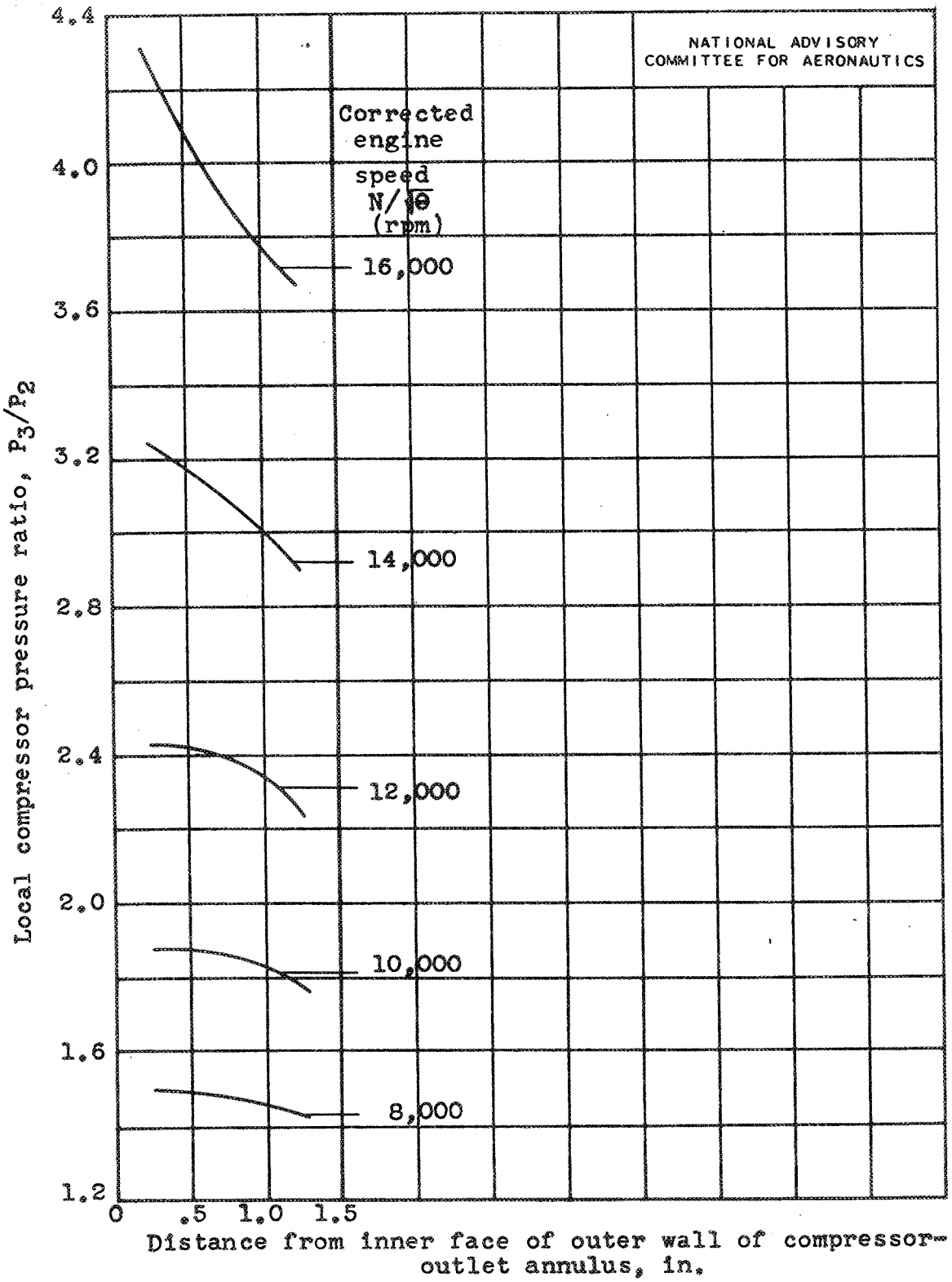

Figure 17.- Total-pressure distribution across compressor-outlet annulus for 19XB-1 turbojet engine as represented by local compressor pressure ratio. Static conditions; simulated altitudes, 5000, 20,000, and 25,000 feet.

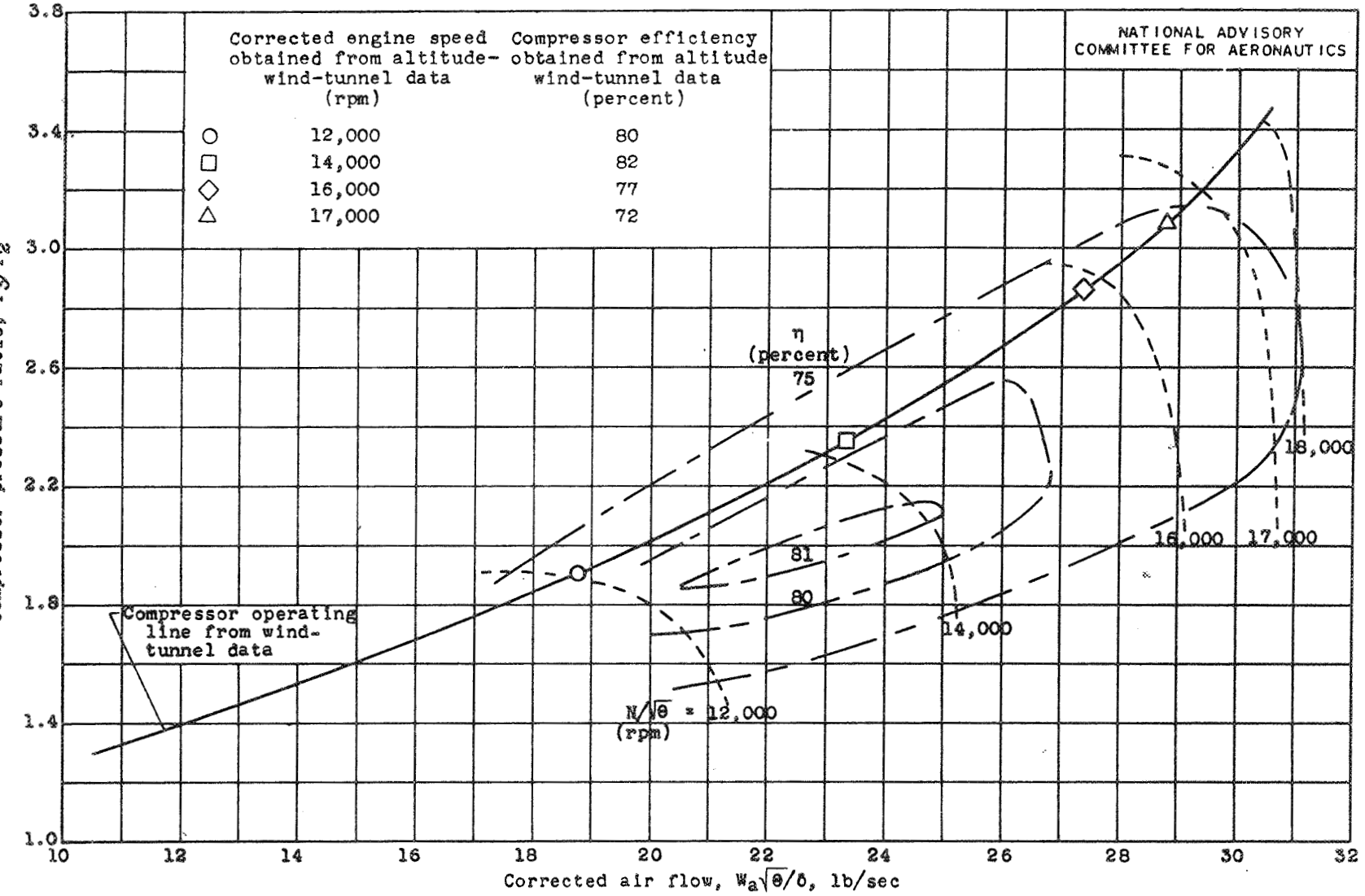

Figure 18.- Comparison of data for 19B compressor obtained in altitude-wind-tunnel investigation of complete engine at static conditions with tail cone in with data obtained in dynamometer tests (reference 4).

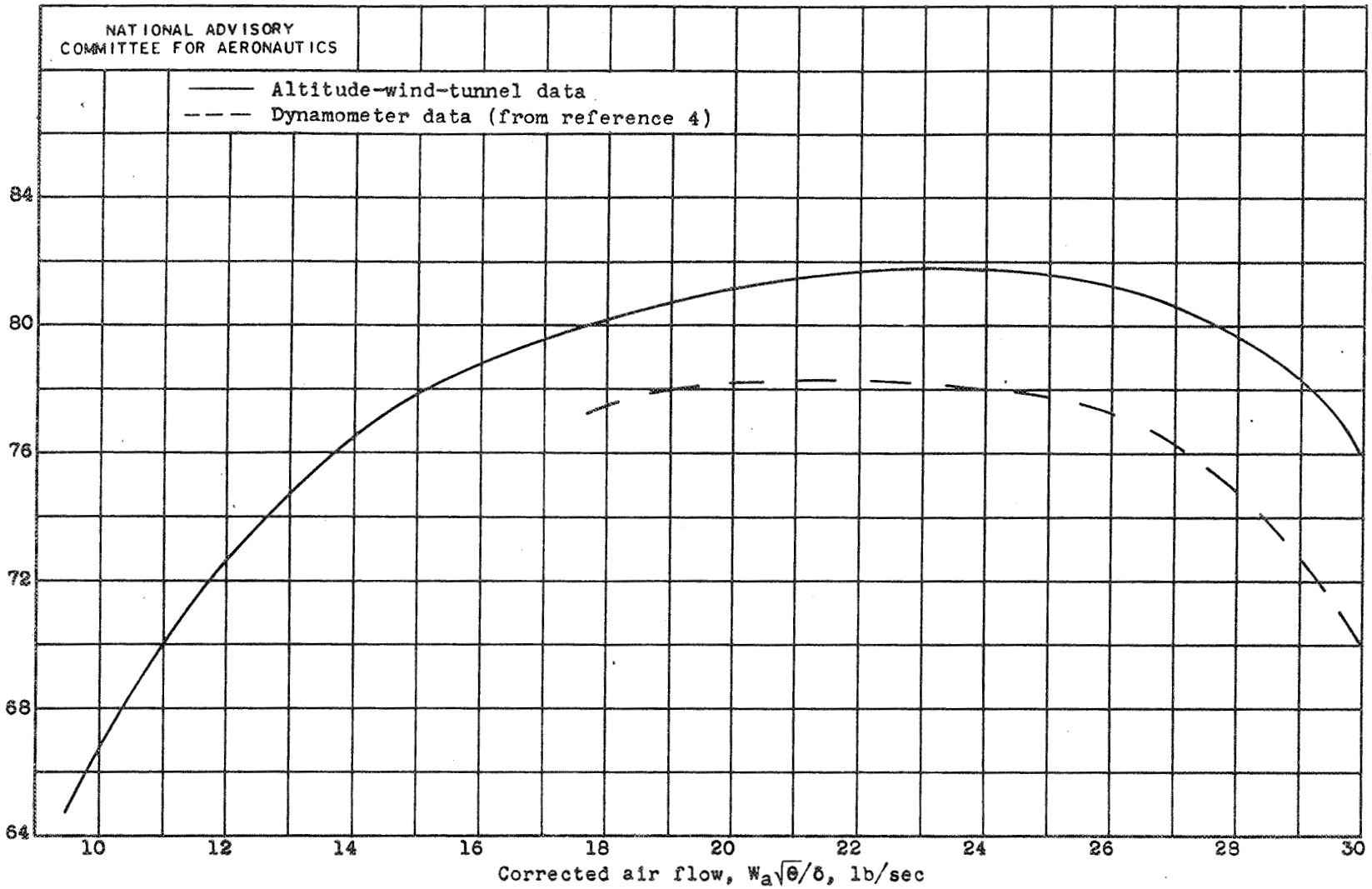

Figure 19.- Comparison of compressor efficiencies for 19B-8 compressor obtained in altitude-wind-tunnel investigation of complete engine with efficiencies obtained in dynamometer tests.